Seasonal Characteristics, Sources and Pollution Pathways of PM$_{10}$ at High Altitudes Himalayas of India

Nikki Choudhary[1,2], Priyanka Srivastava ⓘ [3], Monami Dutta[4], Sauryadeep Mukherjee[4], Akansha Rai[1,2], Jagdish Chandra Kuniyal[5], Renu Lata[6], Abhijit Chatterjee[4], Manish Naja[3], Narayanasamy Vijayan[1,2], Tuhin Kumar Mandal[1,2], Sudhir Kumar Sharma[1,2]*

[1] CSIR-National Physical Laboratory, Dr. K. S. Krishnan Road, New Delhi-110012, India
[2] Academy of Scientific and Innovative Research (AcSIR), Ghaziabad-201002, India
[3] Aryabhatta Research Institute of Observational Sciences (ARIES), Nainital-263002, Uttrakhand, India
[4] Centre for Astroparticle Physics and Space Sciences, Bose Institute, Darjeeling-734102, India
[5] G. B. Pant National Institute of Himalayan Environment, Kosi-Katarmal-263643, Almora, India
[6] G. B. Pant National Institute of Himalayan Environment, Himachal Regional Centre, Mohal-Kullu-175126, India

ABSTRACT

The present study represents the annual and seasonal concentration of PM$_{10}$ over different sites (Darjeeling, Nainital, Mohal-Kullu) across the Himalayan region of India from July 2018 to December 2019. The collected PM$_{10}$ samples were analyzed for carbonaceous aerosols [organic carbon (OC), elemental carbon (EC), water-soluble organic carbon (WSOC), primary organic carbon (POC), secondary organic carbon (SOC)] and major trace elements to inspect their possible sources. The annual average concentrations of PM$_{10}$ over Mohal-Kullu, Nainital, and Darjeeling were recorded as 57 ± 32 µg m^{-3}, 65 ± 41 µg m^{-3}, and 54 ± 17 µg m^{-3}, respectively. The high OC/EC ratio and significant correlation of OC with EC and WSOC with OC indicated a significant effect of biomass burning aerosols over the study sites. Principal component analysis/absolute principal component score (PCA/APCS) resolved four major sources: crustal/soil dust (26.6%), biomass burning/fossil fuel combustion (28%), vehicular emissions (28%), and industrial emissions/coal combustion (17%). Identification of the source region using the potential source contribution function (PSCF) and concentration weighted trajectories (CWT) showed that PM$_{10}$ was mainly transported from the northwestern part of India (Haryana, Punjab), the northeastern region of Pakistan, the Thar Desert, and Indo-Gangetic Plain (IGP), which contributed to dust-related aerosols over the Himalayan region of India.

Keywords: Aerosol, Principal component analysis, Carbonaceous aerosols, Primary organic carbon, Himalayas

1 INTRODUCTION

In recent decades, rising urbanization and booming industrialization have led to the release of various pollutants, predominately particulate matter (PM) (Cheng *et al.*, 2007; Lim and Turpin, 2002). The surge in particle load in the atmosphere has given rise to several environmental (climate change) and human health problems, especially across South Asia (Cheng *et al.*, 2007; Fuzzi *et al.*, 2015; Panwar *et al.*, 2020; Tsai *et al.*, 2012). The concentration and components of aerosols depend on their originating sources, atmospheric processes, and prevailing climatic conditions for the distribution of aerosols (Andreae and Crutzen, 1997; Rastogi and Sarin, 2006).
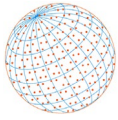
Carbonaceous fractions, the primary constituent of ambient PM, are a source of great concern globally due to their impact on regional and global climate along with the atmospheric system of Earth (Garza *et al.*, 2008; Hansell, 2005; Lim and Turpin, 2002; Phairuang *et al.*, 2020; Ram and Sarin, 2011; Ramanathan and Carmichael, 2008). On the basis of physical and chemical characteristics, carbonaceous aerosols (CAs) are categorized as organic carbon (OC) and elemental carbon (EC). OC is released into the atmosphere from combustion, known as primary OC, or formed by gas-to-particle conversion of volatile organic compounds (VOCs) (referred to as *secondary organic aerosols* [SOA]) (Gupta *et al.*, 2007; Haque *et al.*, 2016; Jimenez *et al.*, 2009) whereas, EC is formed due to the partial combustion (low temperature and low oxygen availability) of carbonaceous fuels. CAs comprise a significant proportion of water-soluble organic carbon (WSOC), function as cloud condensation nuclei (CCN), are hygroscopic, and play a pivotal role in haze formation, posing a health risk (Hegde *et al.*, 2016; Izhar *et al.*, 2019). Besides carbonaceous fractions, PM constitutes various trace elements such as iron, zinc, manganese, and heavy metals such as cadmium, arsenic. Temperature, movement and flow of surface waters, atmospheric circulation, and wind speed all influence the transport of heavy metals and other pollutants (Briffa *et al.*, 2020). Trace metals can adversely impact human health due to their physical presence within the lungs, which hinders gas exchange and allows adsorbed metals to leach into the cells as well as the bloodstream (Baboolal *et al.*, 2020). Heavy metals have high density, atomic weights, or specific gravity (Duffus, 2001; Popoola *et al.*, 2018), and they come into the environment majorly through the deposition of particulates, vehicular emissions, road dust re-suspension, and construction activities (Shrivastav, 2001) causing severe physiological health effects (Bollati *et al.*, 2010; Khillare *et al.*, 2004).

While aerosol chemistry, temporal variation, and source identification have mainly focused on several urban agglomerations across India, therefore, the study of Himalayan aerosols has also piqued the interest of experts (Chatterjee *et al.*, 2021; Gajananda *et al.*, 2005; Kaushal *et al.*, 2018; Kumar and Attri, 2016; Ram *et al.*, 2008; Sarkar *et al.*, 2014, 2015; Sheoran *et al.*, 2021; Soni *et al.*, 2020). The Indian Himalayan Region (IHR) is considered a pristine, ecologically fragile, rich in biodiversity, and highly vulnerable region on Earth (Rai *et al.*, 2021; Yang *et al.*, 2021; Yuan *et al.*, 2020). In addition, urban development raised energy consumption, causing perturbation to the Himalaya's temperature and deteriorating its air quality (Ram and Sarin, 2010; Sharma *et al.*, 2021). Being far from intensive anthropogenic activities, the loading of CAs increases with long-range transport into the IHR along the valleys, accelerating the melting of glaciers by depositing on the snow and ice surface (Yuan *et al.*, 2020, 2021). Previous studies (Cong *et al.*, 2015; Streets *et al.*, 2003; Xu *et al.*, 2018; Yang *et al.*, 2021; Zheng *et al.*, 2017) show that pollutants are transported over the Himalayas during the pre-monsoon season, which coincides with the yearly extreme fire season in South Asia. Therefore, an in-depth study of particle chemistry gives a detailed description of their sources which helps in the development of appropriate mitigation initiatives that may enhance the air quality (Bond *et al.*, 2013; Cao *et al.*, 2006; Pope *et al.*, 2009; Rai *et al.*, 2020; Ramgolam *et al.*, 2009; Sharma *et al.*, 2017, 2018; Ramana *et al.*, 2010). However, only a few studies using receptor models for chemical characterization and source identification have been conducted in the Himalayas (Adak *et al.*, 2014; Panwar *et al.*, 2020; Rai *et al.*, 2020; Sharma *et al.*, 2020a; Sharma *et al.*, 2021; Sheoran *et al.*, 2021; Soni *et al.*, 2020). This study highlights the annual and seasonal variation of PM$_{10}$ (aerodynamic diameter < 10 µm) and its components (carbonaceous and elemental) at Mohal-Kullu, Nainital, and Darjeeling and identifies the possible sources of carbonaceous species and elements of PM$_{10}$ using principal component analysis/absolute principal component scores (PCA/APCS). To identify the specific source regions, we performed the backward trajectory, potential source contribution function (PSCF), and concentration weighted trajectory (CWT). Therefore, the present study on the year-long aerosol chemistry across the Indian Himalayas would undoubtedly be a valuable addition to the existing knowledge and database on atmospheric aerosol pollution.

2 METHODS

2.1 Study Area

The sites were chosen to symbolize the vast stretch of the IHR in the Indian subcontinent, which incorporates the western, central, and eastern regions of the Indian Himalayas, respectively

(Fig. 1). The selected sites represent the combination of local and transboundary features of PM. A brief description of all the study sites is given below:

Mohal-Kullu: The observational site, G. B. Pant 'National Institute of Himalayan Environment' (NIHE), Mohal-Kullu (31.9°N, 77.11°E, 1154 m above sea level (a.s.l.)) situated in the western Himalayan region. As per the microclimatic conditions, the valley is geographically divided into upper and lower valleys. The study site falls under a sub-temperate climate. The lower part of the valley is in the rain shadow zone, which receives the maximum rain during the winter season. The site also experiences heavy snowfall in the winter on the adjacent hilltops but melts within moments due to the increasing temperature (Kuniyal and Guleria, 2010) of the valley. Rapid urbanization over there resulted in increasing tourism and activities related to agro-horticulture. Other activities (biomass burning for residential heating, forest fires, and meteorology) around the experimental site and increased automobile emissions substantially influence the transboundary movement of air masses (Guleria *et al.*, 2012; Kuniyal and Guleria, 2010).

Nainital: The observational site, Aryabhatta Research Institute of Observational Sciences (ARIES), Nainital, is on Manora hill (29.39°N, 79.45°E, 1959 m a.s.l.) in the central Himalayan region. Low altitude mountains encircle this site, the Ganges valley to the southwest, forested areas, and peaking mountains in the northeast region (Fig. 1). The site is sparsely polluted, far from thermal power plants, industries, and immense polluted towns (Dumka *et al.*, 2021; Sagar *et al.*, 2015). The site represents the subtropical highland climatic region of India. Long-range transported dust dominates here during the summer/monsoon months (March–September) due to increased
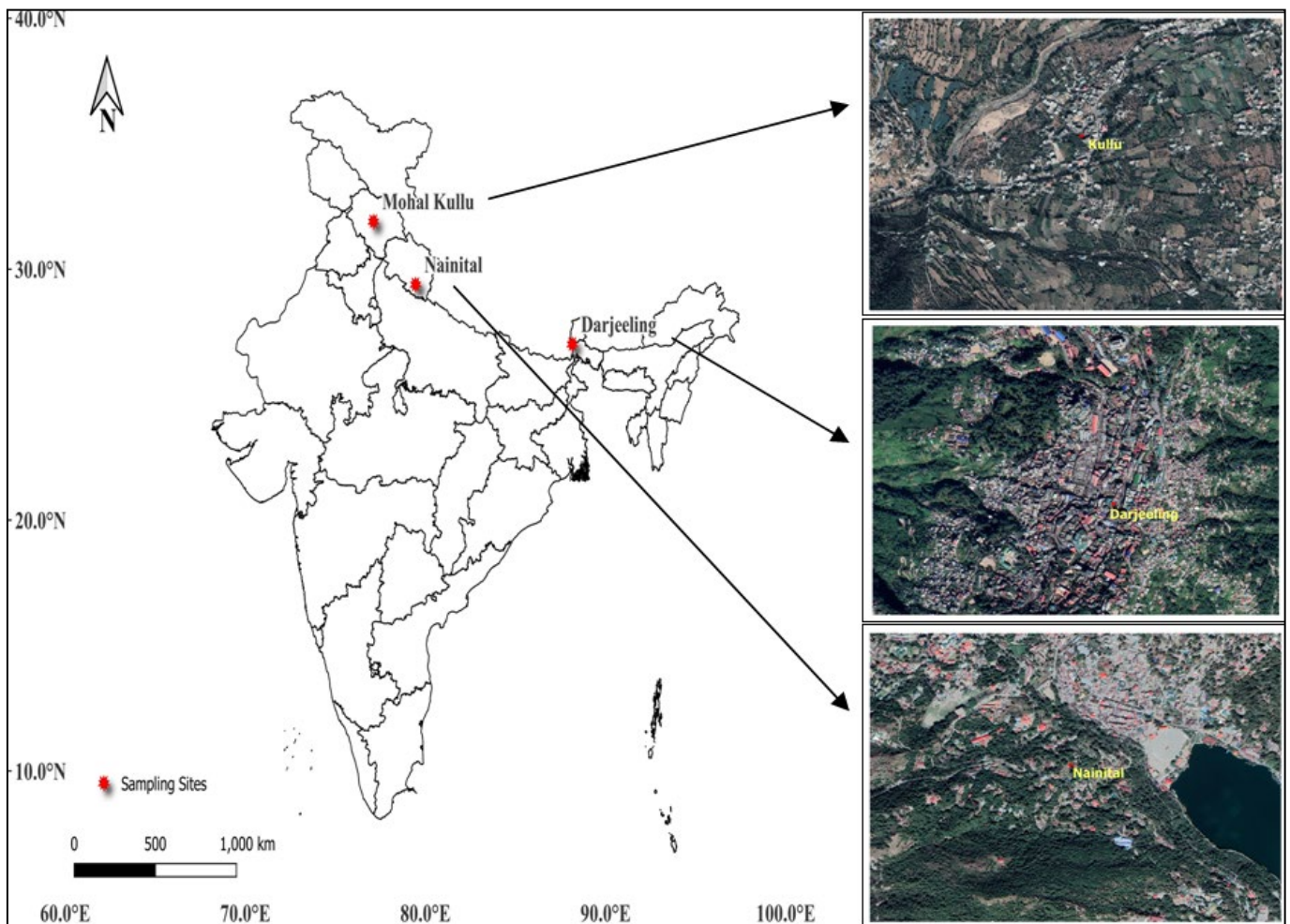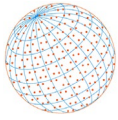

Fig. 1. Topographical map showing the sampling locations (Darjeeling, Nainital, and Mohal-Kullu) over the Himalayan region of India. (Source: Google map)

dust-laden activity over the Thar Desert as well as southwest Asia. During the winter months (January–February), domestic heating increases CAs emissions from wood-burning. A detailed description of the sampling location is discussed in previous studies (Hegde *et al.*, 2016; Naja *et al.*, 2016; Sagar *et al.*, 2015; Sharma *et al.*, 2020b; Sheoran *et al.*, 2021).

Darjeeling: The study site, Bose Institute, Darjeeling (27.01°N, 88.15°E, 2200 m a.s.l.), is located in the eastern Himalayas and surrounded by Nepal, Sikkim, and Bhutan from the west, north, and east sides, respectively. Geographically, Darjeeling is adjacent to the IGP region (a global hotspot for heavy aerosol loadings) (Chatterjee *et al.*, 2021) and is majorly under the influence of tourist activities and biomass burning (Adak *et al.*, 2014). During the monsoon season (June–September), the site has wet summers due to heavy rainfall. A detailed description of weather, topography, and influence of sources on particulate concentrations at the study site are discussed in previous studies (Chatterjee *et al.*, 2021; Rai *et al.*, 2020; Sharma *et al.*, 2021).

Four distinct seasons have been experienced in India [winter (January–February), summer (March–May), monsoon (June–September), and post-monsoon (October–December)] during the year (Rai *et al.*, 2021). These seasons are classified according to India Meteorological Department (IMD).

2.2 Aerosol Sampling

A respirable dust sampler (flow rate: 1.2 m^3 min^{-1}) was used to collect aerosols (24 h) (PM_{10}) on a pre-baked (550°C for 5 h) Pallflex Tissuquartz filters (20 × 25 cm^2) at three urban locations (Bose Institute, Darjeeling; ARIES, Nainital; G. B. Pant NIHE, Mohal-Kullu) from July 2018–December 2019. The pre- (before sampling) and post- (after sampling) weights of the filters were recorded using a weighing balance (resolution: ± 10 μg). The gravimetric mass of PM_{10} was calculated as the difference of post- and pre-filters mass (in μg) divided by the sampled air volume (m^3) passing through the filters. Before the chemical analysis, the filters were kept in a deep freezer at –20°C.

2.3 Chemical Analysis
2.3.1 OC and EC analysis

The OC/EC carbon analyzer (DRI 2001A, Atmoslytic Inc., Calabasas, CA, USA) was used to quantify the OC and EC using the Interagency Monitoring of PROtected Visual Environments (IMPROVE-A) procedure (Chow *et al.*, 2004). The OC/EC analyzer uses a thermal-optical approach that involves volatilization of OC fractions using helium (at 140°C, 280°C, 480°C, and 580°C), followed by oxidation of EC fractions in 98% helium and 2% oxygen (at 580°C, 740°C, and 840°C). A filter punch (~0.536 cm^2 area) was taken from the filter for the analysis. Detailed information on the method used was referenced therein (DRI 2001A user manual; Sharma *et al.*, 2021). In addition, average blank concentrations of OC and EC were determined from the blank filters to correct sample results.
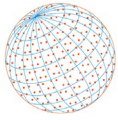
2.3.2 WSOC analysis

A TOC analyzer was used to determine the WSOC in PM_{10} samples (Model: Shimadzu TOC-L CPH/CPN, Japan). The analyzer works on catalytic-oxidation combustion at high temperatures (680°C) to convert OC components into CO_2. The CO_2 was detected using a non-dispersive infrared (NDIR) gas analyzer. A punch size of 30 mm (7.065 cm^2) diameter from PM_{10} was employed for the analysis. Detailed information on the method used to estimate WSOC was discussed in reference therein (Rai *et al.*, 2020; Sharma *et al.*, 2021).

2.3.3 Elemental analysis

We used Wavelength Dispersive X-ray Fluorescence (WD-XRF) Spectrometer (Rigaku ZSX Primus) to determine different elements (Mg, Na, Al, Ca, Fe, Ti, Ni, Cl, S, P, K, Cr, Pb, Cu, Mn, B, Zr, Mo, and Zn) in PM_{10} samples. In addition, the blank filters were analyzed to accurate the intensities for the analyzed sample with repeatability error in the range of 5–10%. The detailed information on the analytical procedure is presented in Sharma *et al.* (2020a).

2.4 Estimation of POC and SOC

The most common method for estimating POC and SOC is the EC tracer method (Mishra and

Kulshrestha, 2021; Srinivas and Sarin, 2014). Both OC and EC are produced by the combustion of fuels, where EC is the primary tracer for POC. $(OC/EC)_{min}$ is the ratio of OC and EC of fresh aerosols emitted during combustion. The following formulas were used to calculate POC and SOC for each season separately:

$$POC = [EC] \times (OC/EC)_{min} \tag{1}$$

$$SOC = OC - POC \tag{2}$$

2.5 Enrichment Factors (EFs)

To delineate the origin of trace metal abundances in aerosols, whether crustal or anthropogenic, EFs have been estimated. The EFs of the elements are computed (Taylor and McLennan, 1995) as:

$$EF = \frac{El_{sample} / X_{sample}}{El_{crust} / X_{crust}} \tag{3}$$

where,
El_{sample} = Elemental concentration.
X_{sample} = Reference element concentration (Al).
El_{crust} = Element concentration in earth crust.
X_{crust} = Reference element concentration in earth crust.

Elements such as Al, Fe, and Ti are widely used as reference materials for calculating the enrichment factor (Taylor and McLennan, 1995). We selected Al (as a reference) element for this study due to its stable and spatially homogeneous distribution in the study area.

2.6 Principal Component Analysis (PCA)/Absolute Principal Component Scores (APCS)

PCA uses the Varimax rotation and orthogonal transformation method to recognize the data patterns. Eigenvalues were restricted to more than 1 for the extracted components. In PCA, the data is normalized using the formula:

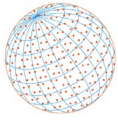$$Z_{ij} = \frac{C_{ij} - \overline{C_J}}{\sigma_j} \tag{4}$$

where i denotes the sample number; j denotes the element number; C_{ij} implies the measured elemental concentration i in j^{th} observation; C_J depicts the arithmetic mean (AM) concentration, and σ_j signifies the standard deviation (SD) for element i. The formulation of the PCA model is as follows:

$$Z_{ij} = \sum_{k=1}^{p} g_{ik} h_{kj} \left(i = 1, 2, ..., m; \ j = 1, 2, ..., p; \ k = 1, 2, ..., n \right) \tag{5}$$

where k denotes the number of sources, h_{kj} and g_{ik} are the factor scores and loadings, respectively (Song et al., 2006). On the basis of factor loading components, each source contribution is estimated using the APCS method (Thurston and Spengler, 1985). For APCS, normalization of PCA results was done using the formula:

$$\left(Z_0 \right)_j = \frac{0 - \overline{C_J}}{\sigma_j} = -\frac{\overline{C_J}}{\sigma_j} \tag{6}$$

After rescaling the scores (known as APCS), linear regression was performed on APCS and the measured concentrations to obtain the accurate source contributions (Song et al., 2006). More

information about PCA/APCS model is found in reference therein (Duan *et al.*, 2006; Guo *et al.*, 2004; Larsen and Baker, 2003; Miller *et al.*, 2002; Thurston and Spengler, 1985).

2.7 Air-Mass Back Trajectory (AMBT) and Probability Functions (PSCF and CWT)

Air-mass backward trajectory (AMBT) has been widely used for the movement of air masses and their long-range transport, which depends on the source and pathway of air masses. We simulated the three days AMBTs using Hybrid Single-Particle Lagrangian Integrated Trajectory (HYSPLIT) model with meteorological data ($1° \times 1°$) of the Global Data Assimilation System (GDAS) (Draxler and Hess, 1998) at different altitudes of 100 m (lower), 500 m (around boundary layer) and 1000 m (higher) above ground level (AGL) (Adak *et al.*, 2014). Different heights were selected to study the significance of transboundary movement and local emission sources, which can interfere with the surface features (buildings) at lower altitudes.

Air parcels contain a specific concentration of pollutants estimated using PSCF (Ashbaugh *et al.*, 1985; Hwang and Hopke, 2007; Li *et al.*, 2017). PSCF divides the potential source region into equal grids of *i* by *j* using Eq. (7):

$$PSCF_{ij} = \frac{m_{ij}}{n_{ij}} \tag{7}$$

n_{ij} denotes the frequency of the trajectories passing each grid cell (*i*, *j*), and m_{ij} denotes the frequency of pollutant concentration exceeding the predefined criteria value (90th percentile of source contribution). A key limitation of the PSCF is that if the sample concentration exceeds the specified percentile, similar PSCF values can be found in multiple grid cells, making it difficult to distinguish between low and high-impact sources. Therefore, CWT addresses this issue by assigning the species concentration and residence time to its corresponding air masses approaching the receptor location (Dumka *et al.*, 2015; Li *et al.*, 2017; Singh *et al.*, 2018).

3 RESULTS AND DISCUSSION

3.1 Annual and Seasonal Variability of PM$_{10}$ and its Carbonaceous Components (OC, EC, WSOC, POC, and TCA)

The annual mean concentration of PM$_{10}$ over Darjeeling (range: 21–116 µg m^{-3}), Nainital (range: 22–250 µg m^{-3}), and Mohal-Kullu (range: 11–173 µg m^{-3}) were found to be 54 ± 17 µg m^{-3}, 65 ± 41 µg m^{-3}, and 57 ± 32 µg m^{-3}, respectively (Table 1). Fig. S1 demonstrates the monthly average mass concentration of PM$_{10}$ over the study sites. The study revealed that the maximum monthly averaged PM$_{10}$ concentration was observed in March (73 µg m^{-3}), May (120 µg m^{-3}), and December (111 µg m^{-3}) over Darjeeling, Nainital, and Mohal-Kullu, respectively. Whereas the minimum monthly averaged PM$_{10}$ concentration was observed in December (39 µg m^{-3}), August (29 µg m^{-3}), and July (15 µg m^{-3}) over Darjeeling, Nainital, and Mohal-Kullu, respectively. Fig. 2 shows the monthly average concentrations of OC, EC, and WSOC in PM$_{10}$ and their mass ratios over the IHR.

Table 1 illustrate the seasonal variation in PM$_{10}$ mass concentrations at Darjeeling, Nainital, and Mohal-Kullu. The highest PM$_{10}$ concentration was recorded in the summer season (March–May) at Darjeeling (63 ± 21 µg m^{-3}) and Nainital (100 ± 50 µg m^{-3}), respectively, which might be due to the mechanism of elevated heat pump that the dust aerosols mixed with CAs primarily from IGP reaches the Himalayan foothills. In addition, the mixed aerosols were vertically advected to higher altitudes and significantly increased the aerosol load over the IHR (Chatterjee *et al.*, 2010; Rai *et al.*, 2021; Sharma *et al.*, 2021). The observed results are in good agreement with the previous studies on Mount Abu (Ram *et al.*, 2008), Manora peak (Hegde *et al.*, 2016; Ram *et al.*, 2008), Mohal-Kullu (Gajananda *et al.*, 2005). On the other hand, the highest PM$_{10}$ concentration over Mohal-Kullu was observed in the post-monsoon season (October–December) (76 ± 36 µg m^{-3}), which may be associated with the shallow atmospheric boundary layer, more influx of tourist vehicles, excess biomass burning activities, and transboundary movement of air masses originated from the IGP region (Gajananda *et al.*, 2005; Ram and Sarin, 2015).
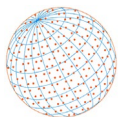
Table 1. Annual and seasonal average variation in concentration of carbonaceous components (OC, EC, WSOC, POC, SOC, TCA) of PM_{10} over different sites of the IHR.

Species	Annual (Jul. 2018–Dec. 2019)	Winter (Jan.–Feb.)	Summer (Mar.–May)	Monsoon (Jun.–Sep.)	Post-monsoon (Oct.–Dec.)
Darjeeling					
PM_{10}	54 ± 17	51 ± 18	63 ± 21	52 ± 12	50 ± 15
OC	5.39 ± 2.24	5.40 ± 2.02	5.18 ± 2.14	3.62 ± 0.87	6.29 ± 2.38
EC	2.31 ± 1.14	2.68 ± 1.00	3.01 ± 1.15	1.15 ± 0.38	2.10 ± 0.96
WSOC	3.59 ± 1.76	3.93 ± 1.29	3.43 ± 2.19	2.31 ± 0.77	4.48 ± 1.53
POC	2.47 ± 1.54	3.41 ± 1.27	3.82 ± 1.46	1.46 ± 0.49	3.62 ± 1.59
SOC	2.94 ± 1.45	1.99 ± 1.10	1.40 ± 0.97	2.15 ± 0.86	2.67 ± 1.22
TCA	10.93 ± 4.47	11.32 ± 4.14	11.29 ± 4.51	6.94 ± 1.55	12.18 ± 4.61
Nainital					
PM_{10}	65 ± 41	38 ± 9	100 ± 50	81 ± 38	47 ± 14
OC	5.27 ± 4.60	2.88 ± 0.98	8.26 ± 1.15	4.32 ± 1.61	4.31 ± 1.33
EC	1.67 ± 1.06	1.32 ± 0.58	2.28 ± 1.43	1.45 ± 0.75	1.42 ± 0.74
WSOC	3.67 ± 2.62	2.05 ± 0.58	5.66 ± 3.47	3.20 ± 1.40	3.01 ± 1.61
POC	2.71 ± 1.71	2.13 ± 0.93	3.69 ± 2.32	2.35 ± 1.21	2.30 ± 1.19
SOC	2.56 ± 3.51	0.75 ± 0.36	4.57 ± 5.59	1.97 ± 1.16	2.02 ± 1.19
TCA	11.11 ± 8.69	6.71 ± 2.45	16.86 ± 13.26	9.24 ± 3.52	9.17 ± 2.95
Mohal-Kullu					
PM_{10}	57 ± 32	51 ± 16	52 ± 15	43 ± 26	76 ± 36
OC	10.76 ± 8.26	11.14 ± 5.33	11.50 ± 6.21	6.54 ± 4.67	15.43 ± 9.96
EC	3.50 ± 1.99	4.23 ± 1.91	3.66 ± 1.54	2.35 ± 1.31	4.67 ± 2.07
WSOC	5.59 ± 3.27	5.32 ± 1.26	4.28 ± 3.00	4.33 ± 1.62	7.49 ± 4.11
POC	6.82 ± 3.87	8.24 ± 3.73	7.13 ± 3.00	4.59 ± 2.56	9.11 ± 4.04
SOC	3.94 ± 4.89	2.90 ± 1.97	4.37 ± 3.37	1.95 ± 2.49	6.33 ± 6.51
TCA	20.71 ± 15.08	22.06 ± 10.39	22.05 ± 11.44	12.82 ± 8.70	29.36 ± 17.84

During the study period, the annual mean concentrations of OC (Darjeeling: 5.39 ± 2.24 μg m⁻³; Nainital: 5.27 ± 4.60 μg m⁻³; Mohal-Kullu: 10.76 ± 8.26 μg m⁻³), EC (Darjeeling: 2.31 ± 1.14 μg m⁻³; Nainital: 1.67 ± 1.06 μg m⁻³; Mohal-Kullu: 3.50 ± 1.99 μg m⁻³), WSOC (Darjeeling: 3.59 ± 1.76 μg m⁻³; Nainital: 3.67 ± 2.62 μg m⁻³), and POC (Darjeeling: 2.47 ± 1.54 μg m⁻³; Nainital: 2.71 ± 1.71 μg m⁻³; Mohal-Kullu: 6.82 ± 3.87 μg m⁻³) were observed (Table 1). Table S1 shows the concentration of PM components (μg m⁻³) at different sites of the IHR.

In the post-monsoon season, we observed the maximum concentration of OC (Darjeeling: 6.29 ± 2.38 μg m⁻³; Mohal-Kullu: 15.43 ± 9.96 μg m⁻³) and WSOC (Darjeeling: 4.48 ± 1.53 μg m⁻³) of PM_{10} (Fig. 3), which might be due to the biomass burning (wood burning) and lowering of the planetary boundary layer (Rai *et al.*, 2021; Ram *et al.*, 2008; Yadav *et al.*, 2013). Nainital has recorded a maximum concentration of OC (8.26 ± 1.15 μg m⁻³) and WSOC (5.66 ± 3.47 μg m⁻³) during the summer season, which shows similarity with previous literature reported over high altitudes (Adhikary *et al.*, 2007; Carrico *et al.*, 2003). High concentration of EC (Darjeeling: 3.01 ± 1.15 μg m⁻³; Nainital: 2.28 ± 1.43 μg m⁻³) and POC (Darjeeling: 3.82 ± 1.46 μg m⁻³; Nainital: 3.69 ± 2.32 μg m⁻³) were found in the summer season. Moreover, higher levels of OC and EC were observed in the post-monsoon and summer seasons, demonstrating the considerable influence of agricultural waste burning followed by rice and wheat harvesting in the northwestern region of the IGP and transborder movement of pollutants to the receptor sites (Chatterjee *et al.*, 2021; Dumka *et al.*, 2015, 2021; Rastogi *et al.*, 2016; Sharma *et al.*, 2021). During the study period, the monsoon season shows the minimum concentration of carbonaceous species in PM_{10}, which might be due to rain-assisted washout (Ram *et al.*, 2008; Sheoran *et al.*, 2021; Yadav *et al.*, 2013).

3.2 OC/EC Ratio and WSOC/OC Ratio

Table 2 highlights the average seasonal ratios of OC/EC and WSOC/OC at each location. In Fig. 2, the monthly average variation in OC/EC and WSOC/OC ratios are reported. Several researchers
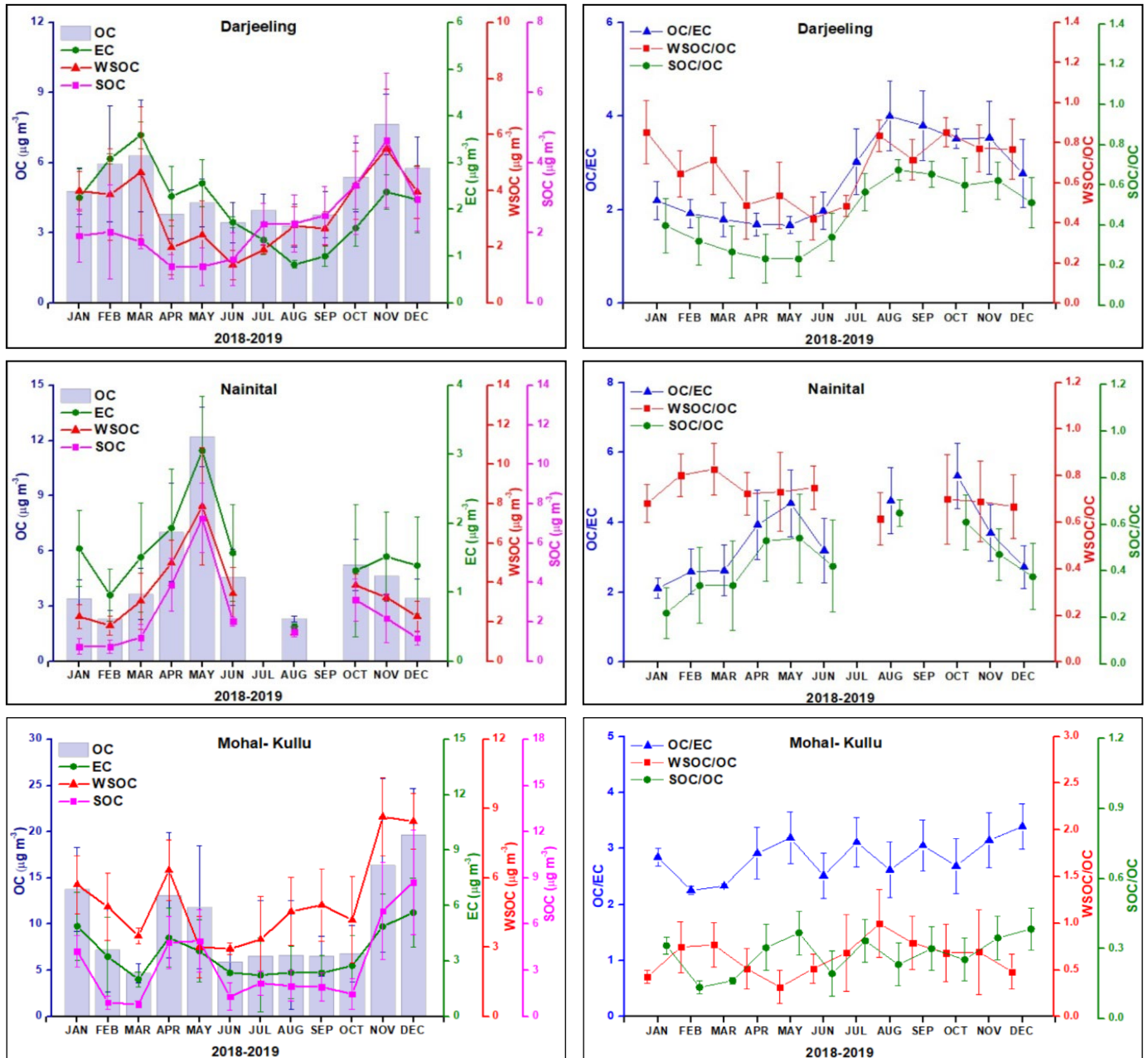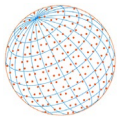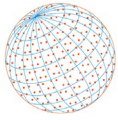
Fig. 2. Monthly average concentrations of OC, EC, and WSOC ($\mu g\ m^{-3}$) in PM_{10} and their mass ratios over different sites in the IHR.

(Andreae and Merlet, 2001; Ram et al., 2008; Saarikoski et al., 2008; Sandradewi et al., 2008; Sudheer and Sarin, 2008) used OC/EC ratio for the identification of CAs sources and differentiate the pollution sources (primary and secondary emissions) which demonstrate higher ratio for biomass burning (BB) and lower for vehicular emission (VE). In this study, the OC/EC ratio exhibited a significant variability, ranging from 1.27 to 6.01 (average: 2.61 ± 1.02) and 1.62 to 10.76 (average: 3.36 ± 1.73) over Darjeeling and Nainital, respectively. The obtained ratios agreed with those reported in the literature (Aggarwal et al., 2012; Ram et al., 2008; Rengarajan et al., 2007; Sharma et al., 2014a, 2014b). The wide range of OC/EC ratios indicates a relatively high fraction of organic aerosols from biomass burning and/or enhanced contribution from SOC formation (Ram and Sarin, 2015; Sheoran et al., 2021). During the winter season, a lower OC/EC ratio (Nainital: 2.33 ± 0.53; Mohal-Kullu: 2.60 ± 0.34) was observed, which is attributable to the dominance of primary organic aerosols from BB (Meng et al., 2018; Ram et al., 2008), whereas Darjeeling shows a lower

OC/EC ratio in the summer season (1.74 ± 0.30) attributable to the formation of SOC (Lim and Turpin, 2002; Ram *et al.*, 2008). The positive linear relationship of OC and EC suggests their emissions from common sources like BB or VE, where EC arises from primary combustion sources,
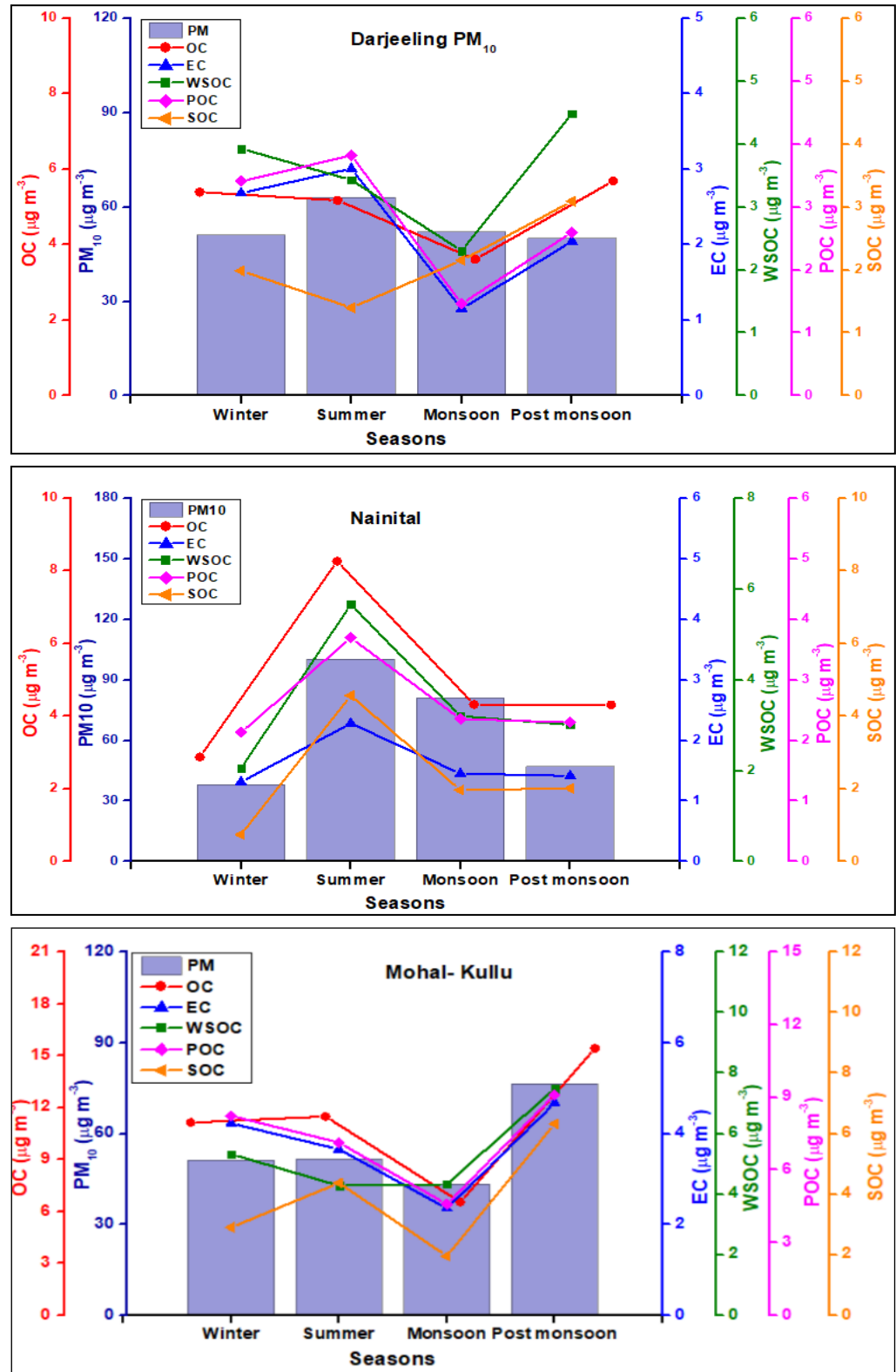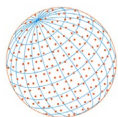

Fig. 3. Seasonal average concentration of carbonaceous components ($\mu g\ m^{-3}$) in PM$_{10}$ at different sites in the IHR.

Table 2. Seasonal average variation in ratios of carbonaceous components (OC, EC, WSOC, SOC) of PM_{10} over different sites of the Himalayan region of India.
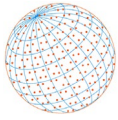
Seasons	Darjeeling			Nainital			Mohal-Kullu		
	OC/EC	WSOC/OC	SOC/OC	OC/EC	WSOC/OC	SOC/OC	OC/EC	WSOC/OC	SOC/OC
Winter (Jan.–Feb.)	2.06 ± 0.37	0.74 ± 0.22	0.36 ± 0.13	2.33 ± 0.53	0.74 ± 0.15	0.28 ± 0.15	2.60 ± 0.34	0.55 ± 0.23	0.24 ± 0.10
Summer (Mar.–May)	1.74 ± 0.30	0.61 ± 0.19	0.25 ± 0.12	3.84 ± 2.20	0.75 ± 0.17	0.48 ± 0.20	2.98 ± 0.62	0.42 ± 0.20	0.32 ± 0.14
Monsoon (Jun.–Sep.)	3.37 ± 1.00	0.65 ± 0.20	0.58 ± 0.15	3.35 ± 1.41	0.73 ± 0.10	0.45 ± 0.20	2.83 ± 0.80	0.84 ± 0.62	0.27 ± 0.16
Post-monsoon (Oct.–Dec.)	3.01 ± 0.85	0.80 ± 0.12	0.54 ± 0.14	3.70 ± 1.93	0.68 ± 0.19	0.47 ± 0.20	3.13 ± 0.80	0.60 ± 0.33	0.33 ± 0.16

which implies that a major proportion of OC also originated from combustion sources (Dewangan et al., 2016; Kumar and Attri, 2016; Ram and Sarin, 2010; Sahu et al., 2018; Salma et al., 2004; Sharma et al., 2020a, 2021). A weak correlation between OC and EC shows that SOA was formed due to the gas-to-particle transformation of VOCs (Begum et al., 2013). Fig. S2 shows the scatter plots of OC and EC for study sites. OC and EC exhibit a significant linear trend during the winter season (Darjeeling: R^2 = 0.765; Nainital: R^2 = 0.854; Mohal-Kullu: R^2 = 0.912). However, in the summer season, the observed samples are widely dispersed (Fig. S2). The well-defined seasonal variability is attributable to the emission potential of sources and the varying contribution from a variety of sources (fossil-fuel combustion (FFC), BB) (Ram et al., 2008; Ram and Sarin, 2015).

The ratio of WSOC/OC is a unique tracer for describing the mechanism of SOA formation (Miyazaki et al., 2009; Ram and Sarin, 2011; Sheoran et al., 2021; Wang et al., 2019). WSOC/OC ratios provide information on chemically processed aerosols, emission processes, hygroscopicity, and atmospheric ageing (Kondo et al., 2007; Zhang et al., 2008). The ratio of WSOC/OC varied from 0.39 to 1.16 (average: 0.72 ± 0.16), and 0.08 to 1.14 (average: 0.70 ± 0.20) over Nainital and Darjeeling, respectively. A high WSOC/OC ratio observed during the summer months (Nainital: 0.75 ± 0.17) attributable to the formation of SOA (Table 2) (Begum et al., 2013; Khare and Baruah, 2010; Ram and Sarin, 2010, 2011; Rengarajan et al., 2007). A similar finding was reported for a high-altitude site in the western Himalayas at the Himansh observatory (average WSOC/OC: 0.60 ± 0.20) (Arun et al., 2019). The high WSOC/OC ratio showed that aged aerosols dominated the central Himalayas and long-distant aerosols from the IGP region (Ram and Sarin, 2015; Sheoran et al., 2021). The scatter plot of WSOC versus OC concentration exhibits a significant correlation in the summer season (Darjeeling: R^2 = 0.905; Nainital: R^2 = 0.797), followed by the post-monsoon, winter, and monsoon season (Table 2), indicating a considerable contribution from SOA (Fig. S2) (Lim and Turpin, 2002; Ram et al., 2008; Ram and Sarin, 2010; Wang et al., 2019).

3.3 Secondary Organic Carbon (SOC)

In Table 1, the mean concentrations of estimated SOC at study sites are reported annually and seasonally. The estimated SOC exhibited an average annual concentration of 2.94 μg m^{-3}, 2.56 μg m^{-3}, and 3.94 μg m^{-3}, corresponding to 54%, 48%, and 36% of the total OC mass over Darjeeling, Nainital, and Mohal-Kullu, respectively. Sheoran et al. (2021) reported the average SOC concentration of 1.99 μg m^{-3} at Nainital, corresponding to 23% of total OC mass. Previous studies (Pachauri et al., 2013; Shivani et al., 2019) reported the percentage contribution of SOC corresponding to total OC mass as 43–49% for $PM_{2.5}$ in urban Delhi and accounted for 18%, 25%, and 60% of OC at traffic, rural, and remote sites, respectively, in Agra. On a seasonal basis, the contribution of SOC corresponding to OC over Darjeeling was highest in the monsoon season (59%), followed by post-monsoon (42%), winter (36%), and summer (27%) season. Whereas for Nainital, the SOC fraction to OC increases in summer (55%) and post-monsoon (46%) season and is lowest in winter (26%) season. Mohal-Kullu showed the highest percentage contribution of SOC to OC in the post-monsoon season (41%) and the lowest in winter (26%). One more study in Delhi reported a 50% contribution of SOC on OC, with the increased value in the summer and winter seasons due to the fast oxidation process and fog processing that affects the formation of

SOC (Rajput et al., 2018; Sheoran et al., 2021). The higher impact of SOC on OC in the summer season than in the winter season can be attributable to intense solar radiation and higher temperature that enhance the photochemical activities and formation of SOC (Cao et al., 2006; Murillo et al., 2013).

3.4 Major and Trace Elements in PM$_{10}$ and their Enrichment Factor (EF)

3.4.1 Concentration of major and trace elements in PM$_{10}$

The mean concentration (annual and seasonal) of major and trace elements of PM$_{10}$ over sampling sites were shown in Tables S2, S3, and S4. Fig. 4 shows the average seasonal concentration of extracted elements in PM$_{10}$ at Darjeeling, Nainital, and Mohal-Kullu. Crustal elements dominate coarse fractions for all sampling sites (Chow et al., 2004). Over Darjeeling, the annual average concentration was observed as maximum for S (1.17 ± 0.7 µg m^{-3}), Al (0.89 ± 0.76 µg m^{-3}), K (0.63 ± 0.35 µg m^{-3}), and Fe (0.61 ± 0.25 µg m^{-3}) (Table S2). Over Nainital, the annual average concentration was observed highest for Ca (1.81 ± 1.88 µg m^{-3}), Al (1.65 ± 1.73 µg m^{-3}), Fe (1.42 ± 1.16 µg m^{-3}), and S (1.35 ± 0.71 µg m^{-3}) (Table S3). Overall, the annual average elemental concentration, along with its percentage contribution to PM$_{10}$, was recorded as 5.24 ± 3.7 µg m^{-3} (10%), 10.03 ± 9.12 µg m^{-3} (15%), and 10.84 ± 8.18 µg m^{-3} (20%) at Darjeeling, Nainital, and Mohal-Kullu, respectively. The seasonal average elemental concentration of PM$_{10}$ was recorded as maximum in the summer season (5.97 ± 3.30 µg m^{-3}) and minimum in the monsoon season (4.85 ± 3.53 µg m^{-3}) over Darjeeling (Fig. 4). Whereas for Nainital, the maximum was observed in the summer season (16.01 ± 10.38 µg m^{-3}) and the minimum in the winter season (6.11 ± 3.28 µg m^{-3}). Das et al. (2013) clearly reported that in the summer season, the dust particles traveled from the western and summer arid regions and accumulated at the foothills of the Himalayas (Soni et al., 2020). Furthermore, for Mohal-Kullu, the maximum was observed in the post-monsoon season (11.04 ± 5.81 µg m^{-3}) and the minimum in the winter season (8.87 ± 2.50 µg m^{-3}).

3.4.2 Enrichment factor (EF)

The elements found in Earth's crust (Al, Fe, Ti, and Ca) are known as crustal elements exhibiting low EFs (< 5) in all seasons at all three sampling sites (Fig. 5). At Darjeeling, EFs of P, Cr, Zn, Pb, Ni, Mo, and B were recorded > 10, indicating their anthropogenic origin in all seasons (Chatterjee et al., 2010). Over Nainital, elements like Zn, Pb, B, Cu, Cr, Zr, Mo, Mn, and Ni showed EF > 10 for all seasons, which indicates their anthropogenic origin. Moreover, the highest EF of B, Mo, Cu, and Ni are attributable to the increased anthropogenic contribution such as industrial emissions (IE) (Shridhar et al., 2009). At Mohal-Kullu, EFs of Mg, Al, Na, Fe, P, Zr, Ca, K, and Sr in PM$_{10}$ were recorded as < 10 in all the seasons, indicating their crustal origin. Moreover, EFs of V, Cr, Ba, and Zn were observed > 10 in all the seasons, indicating their anthropogenic origin.

3.5 Source Apportionment of PM$_{10}$ Using PCA/APCS

SPSS software (IBM, version 26.0) has been used to conduct the PCA analysis. In PCA, Kaiser Normalization and Varimax rotation was applied to maximize the variance of species loadings to identify possible sources of PM$_{10}$. Only principal components (PCs) having greater than 1 eigenvalue were considered in this study.

3.5.1 Darjeeling

In the present study, PCA has been carried out with PM$_{10}$ species to identify the sources using higher factor loadings of PCs. PCA determined four PCs based on factor loadings that explain 69.1% of the total variance (Table 3). The first principal component (PC1) accounts for 30% of the variance that showed the highest loading of Al, Ti, Fe, Ca, Mg, and K, indicating crustal or soil dust (SD) as the primary source (Jain et al., 2017; Jangirh et al., 2022; Shivani et al., 2019). The EFs of the elements showing higher loadings in Factor 1 also confirmed their crustal origin as the significant source of PM$_{10}$ over Darjeeling. Air mass trajectory shows that the continental air masses mainly originated from the northwestern regions of Darjeeling and indicated the resuspension of local and wind-blown soil dust particles for coarse mode aerosols and the influence of biomass burning from fine mode aerosols (Chatterjee et al., 2010). The second component was industrial emissions (IE) + coal combustion (CC), which showed the highest loading of Mg, Ni, Cr, P, Zn, and
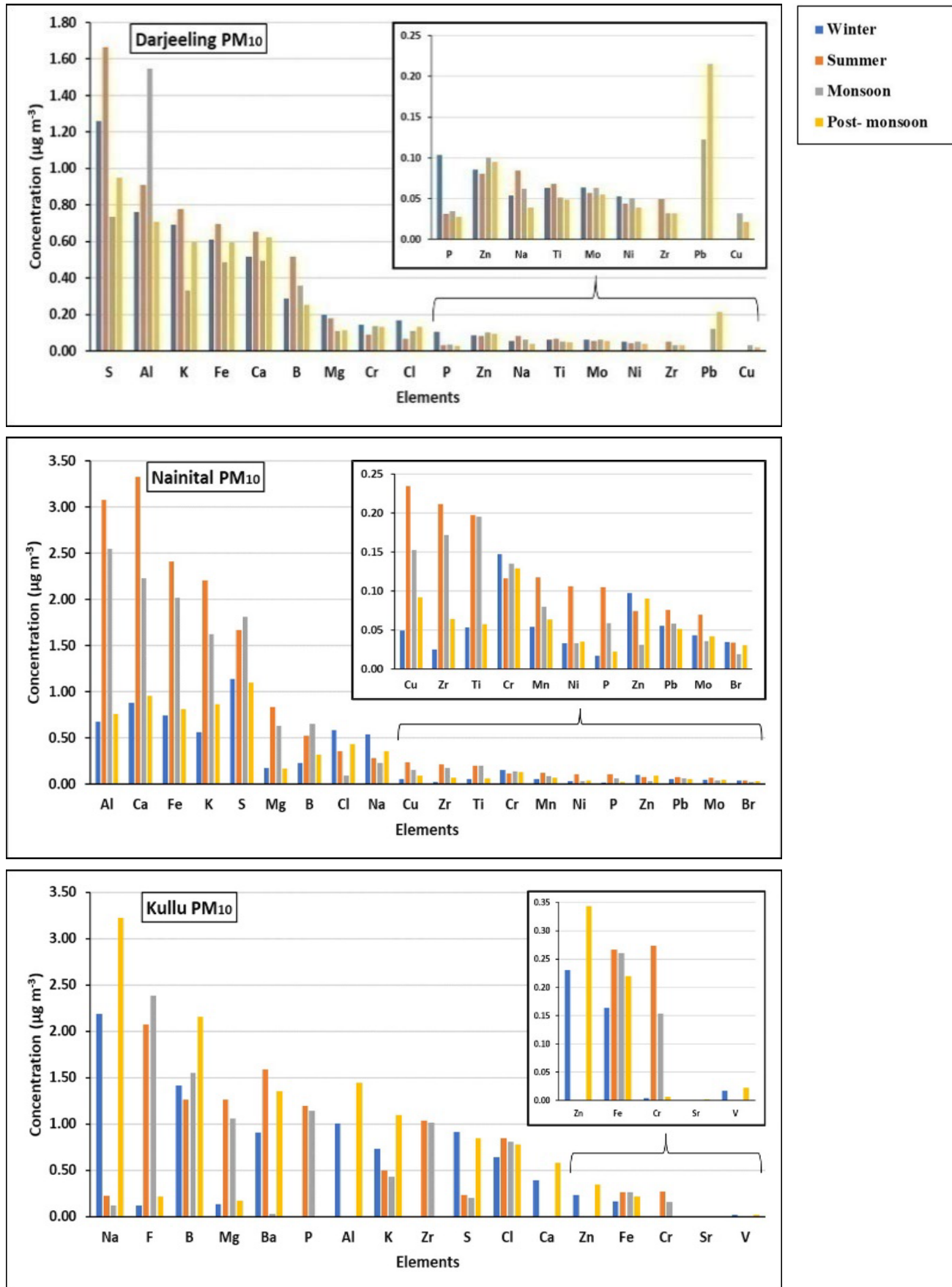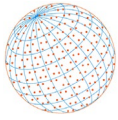
Fig. 4. Seasonal average concentration of elements in PM$_{10}$ at different sites of the IHR.
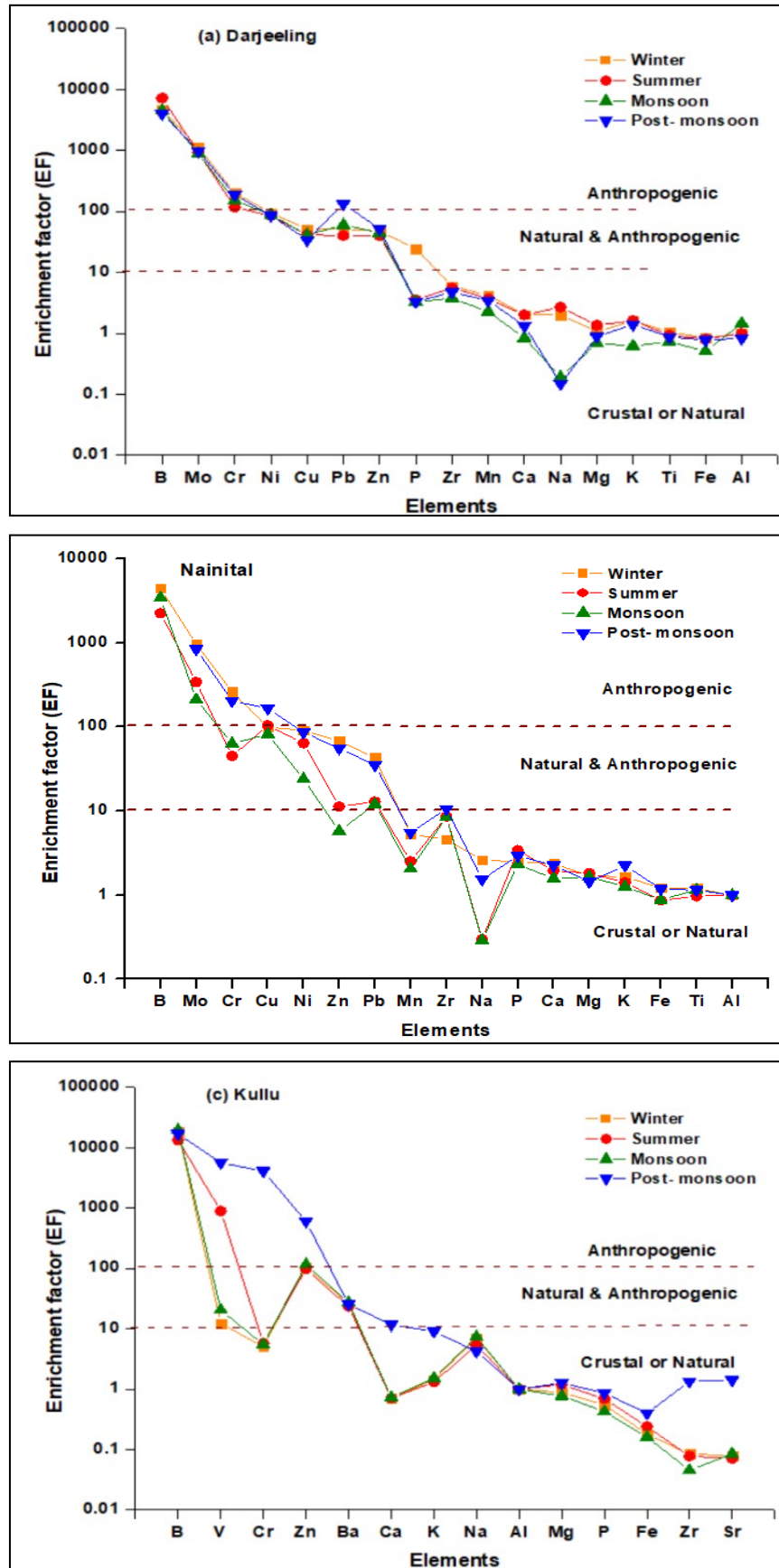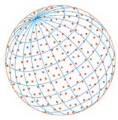
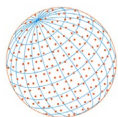**Fig. 5**. Seasonal enrichment factors of PM_{10} at different study sites of the Himalayan region of India.

Table 3. Source profiles obtained from PCA analysis of PM_{10} over different sites in the IHR.

Species	Darjeeling				Nainital				Mohal-Kullu		
	PC1	PC2	PC3	PC4	PC1	PC2	PC3	PC4	PC1	PC2	PC3
OC	-	0.066	**0.840**	0.301	0.569	-	-	**0.483**	**0.576**	0.135	**0.757**
EC	0.064	0.004	**0.894**	**0.797**	0.314	-	-	**0.547**	**0.539**	0.187	**0.728**
WSOC	0.094	0.149	**0.798**	-	0.464	0.408	-	**0.591**	-	-	-
B	0.617	-	0.131	**0.407**	0.085	-	-	**0.875**	**0.935**	0.125	0.297
Na	**0.783**	0.337	0.100	0.236	0.085	-	0.919		**0.961**	0.130	0.228
Mg	0.394	**0.846**	0.173	0.179	**0.920**	0.174	0.123	0.107	0.376	**0.845**	0.330
Al	**0.742**	0.005	-	-	**0.908**	0.291	0.161	0.119	0.082	**0.878**	0.267
P	-	**0.975**	0.026	0.086	**0.761**	**0.585**	0.018	0.066	0.213	**0.892**	0.332
S	**0.509**	-	**0.645**	0.236	0.203	**0.601**	0.182	**0.665**	0.077	**0.880**	**0.654**
Cl	-	**0.801**	0.297	-	0.043	-	**0.440**	**0.450**	0.117	0.129	**0.866**
K	**0.557**	0.120	**0.766**	0.040	0.771	0.381	0.037	**0.575**	**0.924**	0.275	**0.559**
Ca	**0.724**	-	0.183	-	0.844	0.038	**0.441**	-	**0.878**	0.386	0.277
Ti	**0.760**	0.315	0.227	0.051	0.914	0.223	0.131	0.262	-	-	-
Cr	-	**0.948**	-	-	-	-	0.138	0.095	**0.919**	0.276	0.231
Fe	**0.814**	-	0.380	0.025	0.909	0.245	0.225	0.101	0.523	**0.767**	0.320
Ni	0.195	**0.580**	-	-	0.142	0.131	**0.703**	0.161	-	-	-
Cu	0.429	0.050	-	**0.582**	0.481	**0.786**	-	-	-	-	-
Zn	0.421	0.048	0.317	-	-	-	0.272	-	**0.936**	0.263	0.223
Mo	0.091	0.027	-	0.303	-	0.017	-	-	-	-	-
Mn	-	-	-	-	0.592	0.031	-	0.028	-	-	-
Br	-	-	-	-	0.089	0.057	-	-	-	-	-
Zr	0.064	-	0.040	**0.680**	**0.749**	0.050	-	-	0.282	0.106	0.090
Pb	-	-	-	-	0.177	**0.923**	-	-	-	-	-
F	-	-	-	-	-	-	-	-	**0.969**	0.095	0.079
Ba	-	-	-	-	-	-	-	-	**0.938**	0.244	0.235
Sr	-	-	-	-	-	-	-	-	**0.900**	0.212	0.278
Eigenvalues	6.07	3.65	2.61	1.55	11.5	3.0	2.3	1.6	12.7	2.1	1.3
Variance (%)	30.0	18.2	13.0	7.7	48.1	12.6	9.9	7.0	70.6	11.7	7.3
Cumulative Variance (%)	30.0	48.3	61.3	69.1	48.1	60.7	70.6	77.7	70.6	82.3	89.7
Sources	Crustal dust/SD	IE + CC	BB + FFC	VE	Crustal + MD	IE	VE	BB + FFC	VE + IE	Crustal/SD	BB + FFC
% Contribution	10	24	31	35	55	7	13	25	54	15	29

Extraction Method: Principal Component Analysis. Rotation Method: Varimax with Kaiser Normalization. Eigenvalue > 1.00; factor loading $\geq$ 0.40 (highlighted as bold), BB: biomass burning, CC: coal combustion, FFC: fossil fuel combustions, MD: mineral dust, IE: industrial emissions, VE: vehicular emissions; % contribution of sources using APCS.

Cl (Table 3) and contributed 18.2% of the total variance might be originating from small scale coal-based industries and coal engines (Gupta et al., 2007; Jain et al., 2017). Similar results were reported by Chatterjee et al. (2010) that the coal engine used by Darjeeling Himalayan railways is major source of coal combustion markers in Darjeeling. The third source showed the abundance of OC, K, EC, WSOC, S, and Cl in PC3, identified as BB/FFC (Jain et al., 2017; Jangirh et al., 2022; Song et al., 2006), accounting for 13% of the total variance (Table 3), which is also supported by the ratios of OC/EC and WSOC/OC (Sen et al., 2018). At last, the fourth component explains a 7.7% variance with OC, EC, B, and Zr as dominant species, indicating vehicular emissions (VE) as one of the sources primarily due to the massive influx of tourists around the year (Chatterjee et al., 2021).

3.5.2 Nainital

22 chemical constituents of PM_{10} (carbonaceous and elements) have been used to identify the possible sources applying PCA. Four PCs that explain 77.7% of the total variance have been presented in Table 3. The first component explained 48.1% of the variance, and the higher load
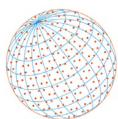
of K, Al, Ti, Mg, Ca, and Fe accredited to crustal + mineral dust source (Balachandran *et al.*, 2000; Jangirh *et al.*, 2022; Khillare *et al.*, 2004; Sheoran *et al.*, 2021). Recent studies (Sharma *et al.*, 2021; Sheoran *et al.*, 2021) reported mineral dust as the major aerosol source over Nainital using PSCF analysis that the major source locations were the Thar desert and desert areas in East Africa (Dumka *et al.*, 2019; Sheoran *et al.*, 2021). As per Fig. 7(b), the southwest monsoon (SWM) that passes the Arabian Sea transports the dust-laden air masses towards the Himalayas. The second factor accredited to the IE with considerable loading of Br, Mn, Ni, Zr, and Zn accounted for 12.6% variance (Chelani *et al.*, 2008; Jain *et al.*, 2019; Pant and Harrison, 2012). The third component, dominated by OC, EC, Ni, and Mn, accounted for 9.9% of the variance attributed to VE (Chakraborty and Gupta, 2010). At last, the fourth component assigned to BB + FFC shows higher loadings of K, OC, S, EC, Cl, and WSOC (Jain *et al.*, 2019; Jangirh *et al.*, 2022; Khare and Baruah, 2010), with 7.2% of the variance. The high OC/EC ratio is also indicative of BB emissions. During the winter season, biomass/wood burning activities enhanced for heating purposes and long-range transport of air masses from BB source areas in Himachal Pradesh, Uttrakhand (forest fires), and Punjab (extensive agricultural BB) is also the major contributor to BB emission markers over Nainital (Sheoran *et al.*, 2021).

3.5.3 Mohal-Kullu

Three components were resolved with a total variance of 89.7%. The first component was dominated by mixed elements attributed to the VE/IE source with a variance of 70.6% (Table 3). Crustal dust sources have been identified in the second component dominated by Mg, Al, P, S, Cl, and Fe, which accounted for 11.7% of the total variance (Table 3) (Jain *et al.*, 2019; Jangirh *et al.*, 2022). At last, the third component was dominated by the marker elements (OC, EC, S, Cl, K), attributed to BB + FFC (Table 3), and accounted for 7.3% of the total variance (Jain *et al.*, 2017; Jangirh *et al.*, 2022; Song *et al.*, 2006).

After PCA, APCS were calculated using factor scores and zero concentration (Larsen and Baker, 2003). Then, linear regression was performed on APCS and measured concentrations of species to estimate the actual source contribution. The measured and predicted PM$_{10}$ concentration using PCA/APCS was depicted in Fig. S4. The predicted species concentration in each source with R^2 was listed in Tables S4–S7 for all sites. Fig. S3 depicts the concentration of chemical species from specific sources determined by APCS. Table S8 reported the identified sources of PM using receptor models over the different sites in the IHR. The percentage contribution of sources were estimated as 10%, 24%, 31%, and 35% for crustal/SD, IE + CC, BB + FFC, and VE, respectively, over Darjeeling (Table 3, Fig. 6). The percentage contribution of sources over Nainital was estimated as 55%, 7%, 13%, and 25% for crustal + mineral dust, IE, VE, and BB + FFC, respectively (Table 3). Over Mohal-Kullu, the estimated percentage contribution of sources was 54%, 15%, 29% for VE + IE, crustal dust/SD, and BB + FFC, respectively (Fig. 6). Majorly the common sources of PM in the IHR are crustal/soil dust/mineral dust, BB/FFC, vehicular activities, and long-range transported aerosols (Table S8). Limited studies are available in the literature to intercompare the identified sources of PM using receptor models (Chatterjee *et al.*, 2010; Panwar *et al.*, 2020; Prabhu *et al.*, 2019; Sheoran *et al.*, 2021; Soni *et al.*, 2020).
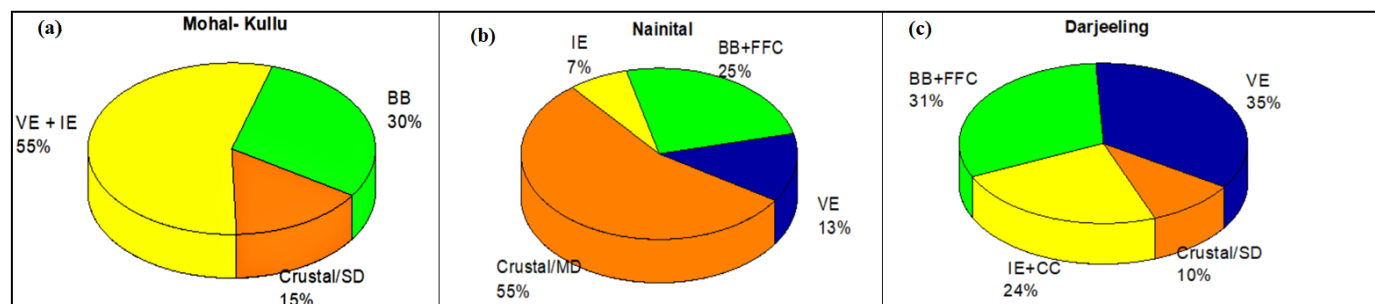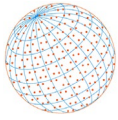

Fig. 6. Percentage contribution of sources over different study sites by PCA/APCS (a) Darjeeling (b) Nainital (c) Mohal-Kullu. (*VE: Vehicular emissions, IE: Industrial emissions, BB: Biomass burning, MD: Mineral dust, FFC: fossil fuel combustion, CC: Coal combustion).

3.6 Influence of Transport Pathway of PM$_{10}$

3.6.1 Backward trajectory

In order to understand the path of particulate air masses reaching the sampling sites, we plotted annual and seasonal AMBTs at all heights (100 m, 500 m, and 1000 m), as shown in Figs. S5 and S6. Annual trajectories at different heights (Fig. S5) for all sites were mainly approaching from the local areas of Uttrakhand, Jammu and Kashmir, the Thar Desert, Himachal Pradesh, Afghanistan, the IGP region, and the Bay of Bengal (BoB). In addition, AMBTs at 500 m AGL for all sampling stations were studied to reduce the surface turbulence impact (Yang *et al.*, 2017).

Fig. 7 depicts the AMBTs at 500 m AGL at all receptor sites originating from local and long-distance regions where the IGP region was the major pollutant emitter. During the summer season, the heavy loadings of AMBTs arriving at Darjeeling (Fig. 7(a)) originated from the semi-arid (the Thar desert, Rajasthan, Punjab) and the IGP region, Assam, Nepal, and Sikkim. Significant transport of AMBTs was observed during the monsoon season, mainly originating from BoB, as reported by (Chatterjee *et al.*, 2021; Rai *et al.*, 2020, 2021). In contrast, local BB activities are a prominent source of PM during the winter season.

During the summer season, the AMBTs arriving at Nainital (Fig. 7(b)) originated from Pakistan, Afghanistan, Iran, the Thar Desert, and the IGP region of India. The IGP region was the major source region during the winter season, where biomass/wood burning activities intensified due to prevailing meteorological conditions (low mixing height and low ambient temperature) (Sharma *et al.*, 2021). Similar to Darjeeling, AMBTs originating from BoB reflected the influence of marine air masses at the receptor site in the monsoon season (Sharma *et al.*, 2021; Sheoran *et al.*, 2021).

During the summer and winter seasons, the AMBTs arriving at Mohal-Kullu (Fig. 7(c)) originated from the local and upper IGP region, Afghanistan, Pakistan, and a few passing over the Arabian Sea. On the other hand, during the post-monsoon season, the heavy loadings of air masses came from northwestern countries (Iran, Afghanistan, Pakistan) (Gajananda *et al.*, 2005).

3.6.2 Potential source contribution function (PSCF)

In order to determine the potential source areas of PM$_{10}$ at the receptor sites (Darjeeling, Nainital, and Mohal-Kullu), the PSCF was done. The grids with a probability < 0.1 are marked as transparent, while other grids are shown in colours (lower probability grids are represented in lighter colours, and higher probability are shown in darker colours). Figs. S7–S10 depicts the annual and seasonal PSCF plots of PM$_{10}$ at all heights (100 m, 500 m, and 1000 m AGL). A detailed description of PSCF results at sampling sites was as follows:

Darjeeling: Overall, heavy loadings of westerly air masses were coming from Rajasthan, Uttar Pradesh, Madhya Pradesh, and other surrounding regions. In the summer season, majorly AMBTs originate from IGP and Nepal region (Ghosh *et al.*, 2021; Rai *et al.*, 2020, 2021), while in the winter as well as post-monsoon season, PSCF shows the source regions are Punjab, Haryana, Himachal Pradesh, Jammu and Kashmir (Fig. S9(a)).

Nainital: During the summer season, most of the air masses approaching the receptor site came from Afghanistan, the Thar Desert, Pakistan, and the IGP region. During the monsoon season, southwest monsoon (SWM) airflows across the Arabian Sea transport dust-laden air masses over the receptor site (Fig. S9(b)). In addition, local biomass/wood burning activities lead to domestic heating in the winter season. In the post-monsoon season, the source regions are Himachal Pradesh, Uttrakhand, Punjab, and nearby areas where extensive agricultural residues burning and forest fires occur, contributing to the long-distance transport of pollutants at the receptor site (Sharma *et al.*, 2021; Sheoran *et al.*, 2021).

Mohal-Kullu: The IGP and the Thar Desert were the primary source region over the receptor site. PSCF plots showed that the dominance of air masses was mainly from the west, northwest, southwest, south, and southeast directions (Fig. S9(c)). AMBTs and its PSCF analysis conclude that the source regions of pollutants are locally-originated from the continental landmass and transboundary movement of air masses (Fig. S9). Though the PSCF analysis successfully recognizes the source regions in the geographical area, the grid cells having a concentration of pollutant greater than the predetermined value have the same PSCF value, and the grid cells which are devoid of any endpoints and known pollution sources could not be considered as source region in this model. Therefore, annual and seasonal CWT was also done for all sampling locations (Figs. S11–S14).
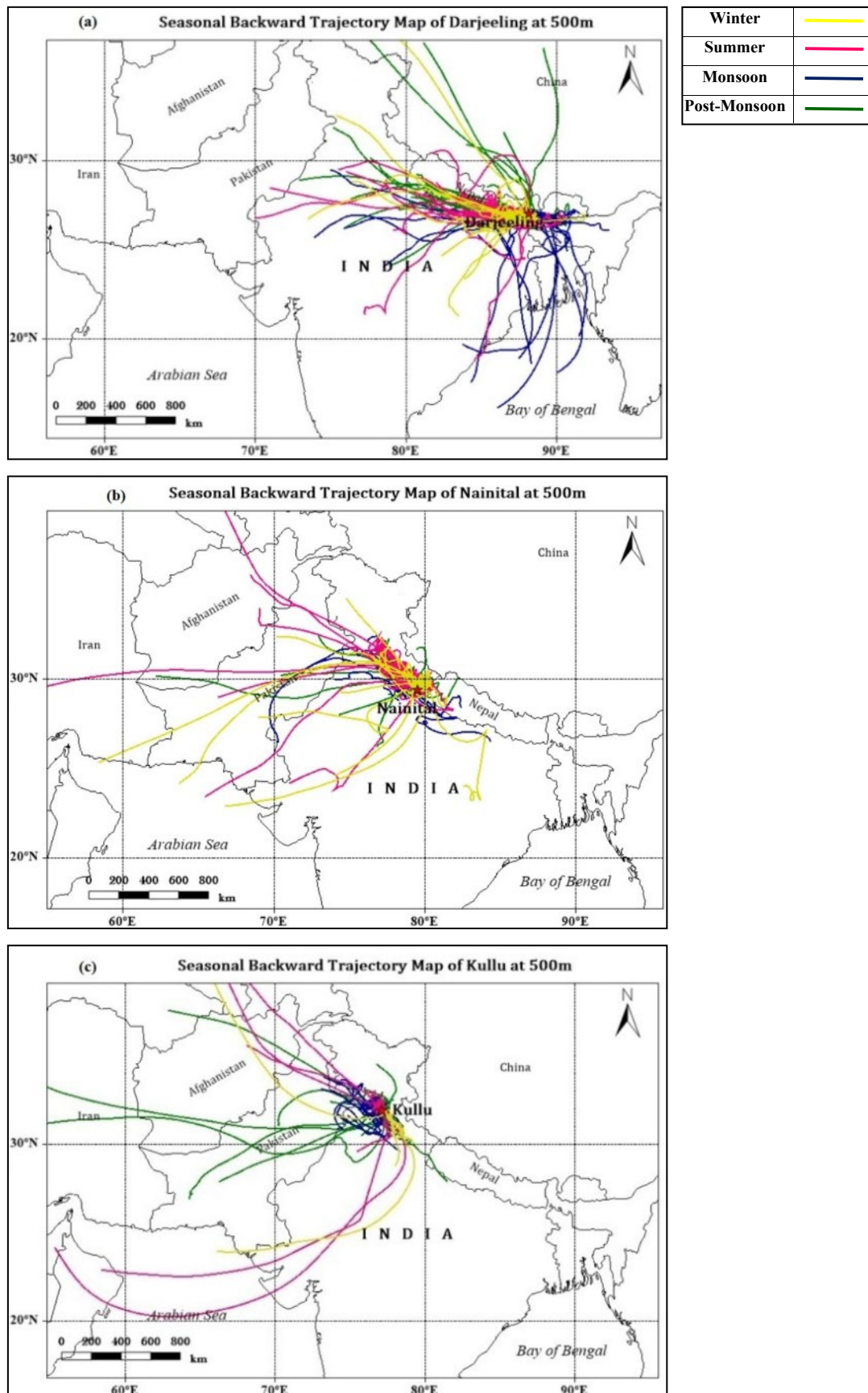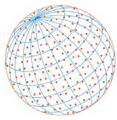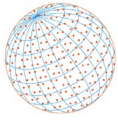
Fig. 7. Seasonal air mass backward trajectories of PM$_{10}$ at the height of 500 m (AGL) over (a) Darjeeling (b) Nainital (c) Mohal-Kullu of India.

3.6.3 Concentration-weighted trajectory (CWT)

CWT calculates the contribution of the source region in terms of PM concentration. Figs. S11–S14 illustrate the annual and seasonal CWT plots of PM$_{10}$ at all heights over each study site. However, measured concentrations of particulates were assigned to grids (termed as hot spots) for CWT analysis. The value of the grid signifies the magnitude of the effect of PM pollution over the observational sites.

Darjeeling: The PM$_{10}$ source regions were mainly local and regional, including the middle and upper IGP region (Fig. S13(a)). The maximum residence duration of AMBTs coming from the IGP region was similar to previous literature (Adak *et al.*, 2014; Sen *et al.*, 2018). During the winter season, Nepal and the IGP region of India contribute maximum to PM concentration, whereas lower CWT originated from the western region and concludes that diverse sources originated from Afghanistan, the Thar Desert, and Pakistan (Rai *et al.*, 2020, 2021; Sharma *et al.*, 2020a). The summer and post-monsoon seasons were considered peak tourism seasons when massive anthropogenic emissions of tourist vehicles and toy trains were observed over the study area. Sen *et al.* (2018) concluded a similar observation that western IGP contributed to particulate concentration in the post-monsoon season due to BB activities for cooking, heating, etc.

Nainital: Fig. S13(b) shows the CWT plot of PM$_{10}$ over Nainital at 500 m (AGL), showing the contribution from the probable source zone with high loadings. During the winter as well as post-monsoon season, the PM sources were primarily local, IGP region, and from neighboring areas of Pakistan. Therefore, the PSCF and trajectory results aligned with the high CWT value, are the potential source areas.
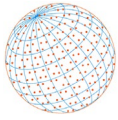
Mohal-Kullu: In all seasons, Fig. S13(c) shows that the significant sources of PM were local regions with higher CWT values. In addition, the long-range transport originated from IGP and nearby areas with lower CWT values.

4 CONCLUSIONS

This study examined the carbonaceous and elemental composition of PM$_{10}$ collected over Darjeeling, Nainital, and Mohal-Kullu from July 2018 to December 2019. Seasonal variation of carbonaceous components and elements in PM$_{10}$ at different sites were assessed to identify the prominent sources (PCA/APCS) of PM$_{10}$ in the high altitude stations of the IHR and their source regions using PSCF and CWT analysis.

Major outcomes of the present study are furnished below:

1. The annual mean concentration of PM$_{10}$ over Nainital, Darjeeling, and Mohal-Kullu was recorded as 65 ± 41 µg m^{-3}, 54 ± 17 µg m^{-3}, and 57 ± 32 µg m^{-3}, respectively. The mass concentration of PM$_{10}$ showed considerable seasonal variability, which might be attributed to long-distance transport of pollutants, local pollution sources, and prevailing climatic conditions.

2. Carbonaceous component concentrations were highest in the winter and post-monsoon seasons (owing to increased burning operations throughout IGP and the Himalayas for household heating) at all three locations. In contrast, the lowest concentration was found during the monsoon season (due to the washout of pollutants).

3. OC/EC ratio and WSOC/OC ratios were used to identify CAs and differentiate the sources as primary and secondary. During the winter season, a low OC/EC ratio is attributable to SOC formation. The high OC/EC ratio and their significant correlation indicate that the BB is one of the major sources in the IHR. WSOC/OC ratio showed that aged aerosols dominated the Himalayan region, and long-range transported aerosols from the IGP region also contributed to PM sources over the Himalayas.

4. The enrichment factor shows the significant contribution of crustal/mineral dust in coarse mode aerosols over the study sites.

5. The PCA revealed four common sources over the IHR: crustal/SD (26.6%), BB + FFC (28%), VE (28%), and IE + CC (17%).

6. PSCF and CWT identified the source areas and showed that PM$_{10}$ was primarily transported from northwestern parts of India (Haryana, Punjab), a northeastern region of Pakistan, and the Thar Desert. In contrast, the IGP and the Thar Desert contributed to dust-related aerosols over the receptor locations.

The findings of this study will be helpful in identifying the specific sources for emission inventories and effectively assessing the climate impacts across Himalayan regions. Further, it is expected that the present study will establish a long-term air quality monitoring network over the Himalayan region of India.

ADDITIONAL INFORMATION AND DECLARATIONS

Author's Contributions

The conceptualization and design of the study were planned by SKS; Data collection and analysis were performed by NC, PS, SM, AR, JCK, RL, AC, NV, MN, TKM, and SKS; the first draft was written by NC. Data interpretation was carried out by NC, SM, JCK, RL, AC, NV, MN, TKM, RKK, and SKS. All the authors read, reviewed, and approved the final manuscript.

Data Availability

The datasets developed during the current study are available from the corresponding author on reasonable request.

Declaration of Competing Interests

The authors declare that they have no conflict of interest.

SUPPLEMENTARY MATERIAL

Supplementary material for this article can be found in the online version at https://doi.org/10.4209/aaqr.220092
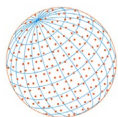
REFERENCES

Adak, A., Chatterjee, A., Singh, A. K., Sarkar, C., Ghosh, S., Raha, S. (2014). Atmospheric fine mode particulates at Eastern Himalaya, India: Role of meteorology, long-range transport and local anthropogenic sources. Aerosol Air Qual. Res. 14, 440–450. https://doi.org/10.4209/aaqr.2013.03.0090

Adhikary, B., Carmichael, G., Tang, Y., Leung, L., Qian, Y., Schauer, J., Stone, E., Ramanathan, V., Ramana, MV (2007). Characterization of the seasonal cycle of south Asian aerosols: A regional-scale modeling analysis. J. Geophys. Res. 112, D22S22. https://doi.org/10.1029/2006JD008143

Aggarwal, S.G., Kawamura, K., Umarji, G.S., Tachibana, E., Patil, R.S., Gupta, P.K. (2012). Organic and inorganic markers and stable C-, N-isotopic compositions of tropical coastal aerosols from
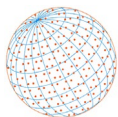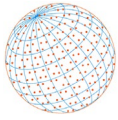
megacity Mumbai: Sources of organic aerosols and atmospheric processing. Atmos. Chem. Phys. 13, 4667–4680. https://doi.org/10.5194/acp-13-4667-2013

Andreae, M.O., Crutzen, P.J. (1997). Atmospheric aerosols: Biogeochemical sources and role in atmospheric chemistry. Science 276, 1052–1058. https://doi.org/10.1126/science.276.5315.1052

Andreae, M.O., Merlet, P. (2001). Emission of trace gases and aerosols from biomass burning. Global Biogeochem. Cycles 15, 955–966. https://doi.org/10.1029/2000GB001382

Arun, B.S., Aswini, A.R., Gogoi, M.M., Hegde, P., Kompalli, S.K., Sharma, P., Babu, S.S. (2019). Physico-chemical and optical properties of aerosols at a background site (4 km a.s.l.) in the western Himalayas. Atmos. Environ. 218, 117017. https://doi.org/10.1016/j.atmosenv.2019.117017

Ashbaugh, L.L., Malm, W.C., Sadeh, W.Z. (1985). A residence time probability analysis of sulfur concentrations at grand Canyon National Park. Atmos. Environ. 19, 1263–1270. https://doi.org/10.1016/0004-6981(85)90256-2

Baboolal, H., Balladin, D., Chadee, S. (2020). Trace metals in fine and respirable ambient air particulates on Trinidad's west coast. J. Geosci. Environ. Protect. 8, 61–81. https://doi.org/10.4236/gep.2020.86006

Balachandran, S., Meena, B., Khillare, P.S. (2000). Particle size distribution and its elemental composition in the ambient air of Delhi. Environ. Int. 26, 49–54. https://doi.org/10.1016/S0160-4120(00)00077-5

Begum, B.A., Hopke, P.K., Markwitz, A. (2013). Air pollution by fine particulate matter in Bangladesh. Atmos. Pollut. Res. 4, 75–86. https://doi.org/10.5094/APR.2013.008

Bollati, V., Marinelli, B., Apostoli, P., Bonzini, M., Nordio, F., Hoxha, M., Pegoraro, V., Motta, V., Tarantini, L., Cantone, L., Schwartz, J., Bertazzi, P.A., Baccarelli, A. (2010). Exposure to metal-rich particulate matter modifies the expression of candidate microRNAs in peripheral blood leukocytes. Environ. Health Perspect. 118, 763–768. https://doi.org/10.1289/ehp.0901300

Bond, T.C., Doherty, S.J., Fahey, D.W., Forster, P.M., Berntsen, T., DeAngelo, B.J., Flanner, M.G., Ghan, S., Kärcher, B., Koch, D., Kinne, S., Kondo, Y., Quinn, P.K., Sarofim, M.C., Schultz, M.G., Schulz, M., Venkataraman, C., Zhang, H., Zhang, S., Bellouin, N., et al. (2013). Bounding the role of black carbon in the climate system: A scientific assessment. J. Geophys. Res. Atmos. 118, 5380–5552. https://doi.org/10.1002/jgrd.50171

Briffa, J., Sinagra, E., Blundell, R. (2020). Heavy metal pollution in the environment and their toxicological effects on humans. Heliyon 6, e04691. https://doi.org/10.1016/j.heliyon.2020.e04691

Cao, J., Lee, S., Ho, K.F., Fung, K., Chow, J., Watson, J. (2006). Characterization of roadside fine particulate carbon and its eight fractions in Hong Kong. Aerosol Air Qual. Res. 6, 106–122. https://doi.org/10.4209/aaqr.2006.06.0001

Carrico, C.M., Kus, P., Rood, M.J., Quinn, P.K., Bates, T.S. (2003). Mixtures of pollution, dust, sea salt, and volcanic aerosol during ACE-Asia: Radiative properties as a function of relative humidity. J. Geophys. Res. 108, 8650. https://doi.org/10.1029/2003JD003405

Chakraborty, A., Gupta, T. (2010). Chemical Characterization and source apportionment of submicron (PM_1) aerosol in Kanpur Region, India. Aerosol Air Qual. Res. 10, 433–445. https://doi.org/10.4209/aaqr.2009.11.0071

Chatterjee, A., Adak, A., Singh, A., Srivastava, M., Ghosh, S., Tiwari, S., Devara, P., Raha, S. (2010). Aerosol Chemistry over a high altitude station at northeastern Himalayas, India. PLoS One 5, e11122. https://doi.org/10.1371/journal.pone.0011122

Chatterjee, A., Mukherjee, S., Dutta, M., Ghosh, A., Ghosh, S.K., Roy, A. (2021). High rise in carbonaceous aerosols under very low anthropogenic emissions over eastern Himalaya, India: Impact of lockdown for COVID-19 outbreak. Atmos. Environ. 244, 117947. https://doi.org/10.1016/j.atmosenv.2020.117947

Chelani, A., Gajghate, D., Devotta, S. (2008). Source apportionment of PM_{10} in Mumbai, India using CMB model. Bull. Environ. Contam. Toxicol. 81, 190–195. https://doi.org/10.1007/s00128-008-9453-2

Cheng, C.T., Wang, W.C., Chen, J.P. (2007). A modeling study of aerosol impacts on cloud microphysics and radiative properties. Q. J. R. Meteorolog. Soc. 133, 283–297. https://doi.org/10.1002/qj.25

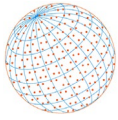Chow, J., Watson, J., Chen, L.W.A., Arnott, W., Moosmuller, H., Fung, K. (2004). Equivalence of

elemental carbon by thermal/optical reflectance and transmittance with different temperature protocols. Environ. Sci. Technol. 38, 4414–4422. https://doi.org/10.1021/es034936u

Cong, Z., Kawamura, K., Kang, S., Fu, P. (2015). Penetration of biomass-burning emissions from South Asia through the Himalayas: New insights from atmospheric organic acids. Sci. Rep. 5, 9580. https://doi.org/10.1038/srep09580

Das, S., Dey, S., Dash, S., Basil, G. (2013). Examining mineral dust transport over the Indian subcontinent using the regional climate model, RegCM4.1. Atmos. Res. 134, 64–76. https://doi.org/10.1016/j.atmosres.2013.07.019

Dewangan, S., Pervez, S., Chakrabarty, R., Watson, J., Chow, J., Pervez, Y., Tiwari, S., Rai, J. (2016). Study of carbonaceous fractions associated with indoor $PM_{2.5}/PM_{10}$ during Asian cultural and ritual burning practices. Build. Environ. 106, 229–236. https://doi.org/10.1016/j.buildenv.2016.06.006

Draxler, R., Hess, G. (1998). An overview of the HYSPLIT_4 modeling system for trajectories, dispersion, and deposition. Aust. Meteorol. Mag. 47, 295–308.

Duan, F., He, K., Ma, Y., Yang, F., Yu, X., Cadle, S., Chan, T.T., Mulawa, P. (2006). Concentration and chemical characteristics of $PM_{2.5}$ in Beijing, China: 2001-2002. Sci. Total Environ. 355, 264–275. https://doi.org/10.1016/j.scitotenv.2005.03.001

Duffus, J.H. (2001). "Heavy metals"–A meaningless term. Chem. Int. 23, 163–167. https://doi.org/10.1515/ci.2001.23.6.163

Dumka, U.C., Kaskaoutis, D.G., Srivastava, M.K., Devara, P.C.S. (2015). Scattering and absorption properties of near-surface aerosol over Gangetic–Himalayan region: The role of boundary-layer dynamics and long-range transport. Atmos. Chem. Phys. 15, 1555–1572. https://doi.org/10.5194/acp-15-1555-2015

Dumka, U.C., Kaskaoutis, D.G., Francis, D., Chaboureau, J.P., Rashki, A., Tiwari, S., Singh, S., Liakakou, E., Mihalopoulos, N. (2019). The role of the intertropical discontinuity region and the heat low in dust emission and transport over the thar desert, India: A premonsoon case study. J. Geophys. Res. 124, 13197–13219. https://doi.org/10.1029/2019JD030836

Dumka, U.C., Kaskaoutis, D.G., Mihalopoulos, N., Sheoran, R. (2021). Identification of key aerosol types and mixing states in the central Indian Himalayas during the GVAX campaign: The role of particle size in aerosol classification. Sci. Total Environ. 761, 143188. https://doi.org/10.1016/j.scitotenv.2020.143188

Fuzzi, S., Baltensperger, U., Carslaw, K., Decesari, S., Denier van der Gon, H., Facchini, M.C., Fowler, D., Koren, I., Langford, B., Lohmann, U., Nemitz, E., Pandis, S., Riipinen, I., Rudich, Y., Schaap, M., Slowik, J.G., Spracklen, D.V., Vignati, E., Wild, M., Williams, M., *et al.* (2015). Particulate matter, air quality and climate: lessons learned and future needs. Atmos. Chem. Phys. 15, 8217–8299. https://doi.org/10.5194/acp-15-8217-2015

Gajananda, K., Kuniyal, J.C., Momin, G., Pasumarti, R., Safai, P., Tiwari, S., Ali, K. (2005). Trend of atmospheric aerosols over the north western Himalayan region, India. Atmos. Enviro. 39, 4817–4825. https://doi.org/10.1016/j.atmosenv.2005.01.038

Garza, K., Soto, K., Murr, L. (2008). Cytoxicity and reactive oxygen species generation from aggregated carbon and carbonaceous nanoparticulate materials. Int. J. Nanomed. 3, 83–94. https://doi.org/10.2147/IJN.S2464

Ghosh, A., Patel, A., Rastogi, N., Sharma, S.K., Mandal, T.K., Chatterjee, A. (2021). Size-segregated aerosols over a high altitude Himalayan and a tropical urban metropolis in Eastern India: Chemical characterization, light absorption, role of meteorology and long range transport. Atmos. Environ. 254, 118398. https://doi.org/10.1016/j.atmosenv.2021.118398

Guleria, R.P., Kuniyal, J.C., Sharma, N.L., Dhyani, P.P. (2012). Seasonal variability in aerosol optical and physical characteristics estimated using the application of the Ångström formula over Mohal in the northwestern Himalaya, India. J. Earth Syst. Sci. 121, 697–710. https://doi.org/10.1007/s12040-012-0194-6

Guo, H., Wang, T., Louie, P.K.K. (2004). Source apportionment of ambient non-methane hydrocarbons in Hong Kong: Application of a principal component analysis/absolute principal component scores (PCA/APCS) receptor model. Environ. Pollut. 129, 489–498. https://doi.org/10.1016/j.envpol.2003.11.006

Gupta, A.K., Karar, K., Srivastava, A. (2007). Chemical mass balance source apportionment of PM_{10} and TSP in residential and industrial sites of an urban region of Kolkata, India. J. Hazard.
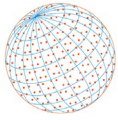
Mater. 142, 279–287. https://doi.org/10.1016/j.jhazmat.2006.08.013

Hansell, D.A. (2005). Dissolved Organic Carbon Reference Material Program. Eos Trans. AGU 86, 318. https://doi.org/10.1029/2005EO350003

Haque, M.M., Kawamura, K., Kim, Y. (2016). Seasonal variations of biogenic secondary organic aerosol tracers in ambient aerosols from Alaska. Atmos. Environ. 130, 95–104. https://doi.org/10.1016/j.atmosenv.2015.09.075

Hegde, P., Kawamura, K., Joshi, H., Naja, M. (2016). Organic and inorganic components of aerosols over the central Himalayas: Winter and summer variations in stable carbon and nitrogen isotopic composition. Environ. Sci. Pollut. Res. 23, 6102–6118. https://doi.org/10.1007/s11356-015-5530-3

Hwang, I., Hopke, P. (2007). Estimation of source apportionment and potential source locations of $PM_{2.5}$ at a west coastal IMPROVE site. Atmos. Environ. 41, 506–518. https://doi.org/10.1016/j.atmosenv.2006.08.043

Izhar, S., Gupta, T., Panday, A. (2019). Scavenging efficiency of water soluble inorganic and organic aerosols by fog droplets in the Indo Gangetic Plain. Atmos. Res. 235, 104767. https://doi.org/10.1016/j.atmosres.2019.104767

Jain, S., Sharma, S.K., Choudhary, N., Masiwal, R., Saxena, M., Sharma, A., Mandal, T.K., Gupta, A., Gupta, N.C., Sharma, C. (2017). Chemical characteristics and source apportionment of $PM_{2.5}$ using PCA/APCS, UNMIX, and PMF at an urban site of Delhi, India. Environ. Sci. Pollut. Res. 24, 14637–14656. https://doi.org/10.1007/s11356-017-8925-5

Jain, S., Sharma, S.K., Srivastava, M.K., Chaterjee, A., Singh, R.K., Saxena, M., Mandal, T.K. (2019). Source apportionment of PM_{10} over three tropical urban atmospheres at Indo-Gangetic Plain of India: An approach using different receptor models. Arch. Environ. Contam. Toxicol. 76, 114–128. https://doi.org/10.1007/s00244-018-0572-4

Jangirh, R., Ahlawat, S., Arya, R., Mondal, A., Yadav, L., Kotnala, G., Yadav, P., Choudhary, N., Rani, M., Banoo, R., Rai, A., Saharan, U.S., Rastogi, N., Patel, A., Shivani, Gadi, R., Saxena, P., Vijayan, N., Sharma, C., Sharma, S.K., *et al.* (2022). Gridded distribution of total suspended particulate matter (TSP) and their chemical characterization over Delhi during winter. Environ. Sci. Pollut. Res. 29, 17892–17918. https://doi.org/10.1007/s11356-021-16572-w

Jimenez, J.L., Canagaratna, M.R., Donahue, N.M., Prevot, A.S.H., Zhang, Q., Kroll, J.H., DeCarlo, P.F., Allan, J.D., Coe, H., Ng, N.L., Aiken, A.C., Docherty, K.S., Ulbrich, I.M., Grieshop, A.P., Robinson, A.L., Duplissy, J., Smith, J.D., Wilson, K.R., Lanz, V.A., Hueglin, C., *et al.* (2009). Evolution of organic aerosols in the atmosphere. Science 326, 1525–1529. https://doi.org/10.1126/science.1180353

Kaushal, D., Kumar, A., Yadav, S., Tandon, A., Attri, A. (2018). Wintertime carbonaceous aerosols over Dhauladhar region of North-Western Himalayas. Environ. Sci. Pollut. Res. 25, 8044–8056. https://doi.org/10.1007/s11356-017-1060-5

Khare, P., Baruah, BP (2010). Elemental characterization and source identification of $PM_{2.5}$ using multivariate analysis at the suburban site of North-East India. Atmos. Res. 98, 148–162. https://doi.org/10.1016/j.atmosres.2010.07.001

Khillare, P.S., Balachandran, S., Meena, B. (2004). Spatial and temporal variation of heavy metals in atmospheric aerosol of Delhi. Environ. Monit. Assess. 90, 1–21. https://doi.org/10.1023/B:EMAS.0000003555.36394.17

Kondo, Y., Miyazaki, Y., Takegawa, N., Miyakawa, T., Weber, R.J., Jimenez, J.L., Zhang, Q., Worsnop, D.R. (2007). Oxygenated and water-soluble organic aerosols in Tokyo. J. Geophys. Res. 112, D01203. https://doi.org/10.1029/2006JD007056

Kumar, A., Attri, A. (2016). Biomass combustion a dominant source of carbonaceous aerosols in the ambient environment of western Himalayas. Aerosol Air Qual. Res. 16, 519–529. https://doi.org/10.4209/aaqr.2015.05.0284

Kuniyal, J.C., Guleria, R. (2010, January). Aerosols optical properties prone to climate change over Mohal-Kullu in the northwestern Himalaya, India. Conference of Indian Aerosol Science and Technology Association on: Aerosols and clouds: Climate Change perspective, Bose institute Darjeeling, India, March 24-26, 19(1 and 2), pp. 227–230.

Larsen, R., Baker, J. (2003). Source apportionment of polycyclic aromatic hydrocarbons in the urban atmosphere: A comparison of three methods. Environ. Sci. Technol. 37, 1873–1881. https://doi.org/10.1021/es0206184

Li, D., Liu, J., Zhang, J., Gui, H., Du, P., Yu, T., Wang, J., Lu, Y., Liu, W., Cheng, Y. (2017). Identification of long-range transport pathways and potential sources of PM$_{2.5}$ and PM$_{10}$ in Beijing from 2014 to 2015. J. Environ. Sci. 56, 214–229. https://doi.org/10.1016/j.jes.2016.06.035

Lim, H.J., Turpin, B.J. (2002). Origins of primary and secondary organic aerosol in Atlanta: Results of time-resolved measurements during the Atlanta supersite experiment. Environ. Sci. Technol. 36, 4489–4496. https://doi.org/10.1021/es0206487

Meng, X., Garay, M.J., Diner, D.J., Kalashnikova, O.V., Xu, J., Liu, Y. (2018). Estimating PM$_{2.5}$ speciation concentrations using prototype 4.4 km-resolution MISR aerosol properties over Southern California. Atmos. Environ. 181, 70–81. https://doi.org/10.1016/j.atmosenv.2018.03.019

Miller, S., Anderson, M., Daly, E., Milford, J. (2002). Source apportionment of exposures to volatile organic compounds. I. Evaluation of receptor models using simulated exposure data. Atmos. Environ. 36, 3629–3641. https://doi.org/10.1016/S1352-2310(02)00279-0

Mishra, M., Kulshrestha, U.C. (2021). Source impact analysis using char-EC/Soot-EC ratios in the central Indo-Gangetic Plain (IGP) of India. Aerosol Air Qual. Res. 21, 200628. https://doi.org/10.4209/aaqr.200628

Miyazaki, Y., Kondo, Y., Shiraiwa, M., Takegawa, N., Miyakawa, T., Han, S., Kita, K., Hu, M., Deng, Z.Q., Zhao, Y., Sugimoto, N., Blake, D.R., Weber, R.J. (2009). Chemical characterization of water-soluble organic carbon aerosols at a rural site in the Pearl River Delta, China, in the summer of 2006. J. Geophys. Res. 114, D14208. https://doi.org/10.1029/2009JD011736

Murillo, J.H., Roman, S.R., Marin, J.F.R., Ramos, A.C., Jimenez, S.B., Gonzalez, B.C., Baumgardner, D.G. (2013). Chemical characterization and source apportionment of PM$_{10}$ and PM$_{2.5}$ in the metropolitan area of Costa Rica, Central America. Atmos. Pollut. Res. 4, 181–190. https://doi.org/10.5094/APR.2013.018

Naja, M., Bhardwaj, P., Singh, N., Kumar, P., Kumar, R., Ojha, N., Sagar, R., Satheesh, S., Moorthy, K.K., Kotamarthi, V. (2016). SPECIAL SECTION: RAWEX–GVAX: High-frequency vertical profiling of meteorological parameters using AMF1 facility during RAWEX–GVAX at ARIES, Nainital. Curr. Sci. 111, 132–140. https://doi.org/10.18520/cs/v111/i1/132-140

Pachauri, T., Singla, V., Satsangi, A., Lakhani, A., Kumari, K.M. (2013). Characterization of carbonaceous aerosols with special reference to episodic events at Agra, India. Atmos. Res. 128, 98–110. https://doi.org/10.1016/j.atmosres.2013.03.010

Pant, P., Harrison, R. (2012). Critical review of receptor modelling for particulate matter: A case study of India. Atmos. Environ. 49, 1–12. https://doi.org/10.1016/j.atmosenv.2011.11.060

Panwar, P., Prabhu, V., Soni, A., Punetha, D., Shridhar, V. (2020). Sources and health risks of atmospheric particulate matter at Bhagwanpur, an industrial site along the Himalayan foothills. SN Appl. Sci. 2, 632. https://doi.org/10.1007/s42452-020-2420-1

Phairuang, W., Inerb, M., Furuuchi, M., Hata, M., Tekasakul, S., Tekasakul, P. (2020). Size-fractionated carbonaceous aerosols down to PM$_{0.1}$ in southern Thailand: Local and long-range transport effects. Environ. Pollut. 260, 114031. https://doi.org/10.1016/j.envpol.2020.114031

Pope, C.A., Ezzati, M., Dockery, D.W. (2009). Fine-particulate air pollution and life expectancy in the United States. N. Engl. J. Med. 360, 376–386. https://doi.org/10.1056/NEJMsa0805646

Popoola, L.T., Adebanjo, S.A., Adeoye, B.K. (2018). Assessment of atmospheric particulate matter and heavy metals: A critical review. Int. J. Environ. Sci. Technol. 15, 935–948. https://doi.org/10.1007/s13762-017-1454-4

Prabhu, V., Shridhar, V., Choudhary, A. (2019). Investigation of the source, morphology, and trace elements associated with atmospheric PM$_{10}$ and human health risks due to inhalation of carcinogenic elements at Dehradun, an Indo-Himalayan city. SN Appl. Sci. 1, 429. https://doi.org/10.1007/s42452-019-0460-1

Rai, A., Mukherjee, S., Chatterjee, A., Choudhary, N., Kotnala, G., Mandal, T., Sharma, S.K. (2020). Seasonal variation of OC, EC, and WSOC of PM$_{10}$ and their cwt Analysis over the eastern Himalaya. Aerosol Sci. Eng. 4, 26–40. https://doi.org/10.1007/s41810-020-00053-7

Rai, A., Mukherjee, S., Choudhary, N., Ghosh, A., Chatterjee, A., Mandal, T., Sharma, S.K., Kotnala, R. (2021). Seasonal transport pathway and sources of carbonaceous aerosols at an urban site of eastern Himalaya. Aerosol Sci. Eng. 5, 318–343. https://doi.org/10.1007/s41810-021-00106-5

Rajput, P., Singh, D., Singh, A., Gupta, T. (2018). Chemical composition and source-apportionment

of sub-micron particles during wintertime over Northern India: New insights on influence of fog-processing. Environ. Pollut. 233, 81–91. https://doi.org/10.1016/j.envpol.2017.10.036

Ram, K., Sarin, M.M., Hegde, P. (2008). Atmospheric abundances of primary and secondary carbonaceous species at two high-altitude sites in India: Sources and temporal variability. Atmos. Environ. 42, 6785–6796. https://doi.org/10.1016/j.atmosenv.2008.05.031

Ram, K., Sarin, M.M. (2010). Spatio-temporal variability in atmospheric abundances of EC, OC and WSOC over Northern India. J. Aerosol Sci. 41, 88–98. https://doi.org/10.1016/j.jaerosci.2009.11.004

Ram, K., Sarin, M.M. (2011). Day–night variability of EC, OC, WSOC and inorganic ions in urban environment of Indo-Gangetic Plain: Implications to secondary aerosol formation. Atmos. Environ. 460–468. https://doi.org/10.1016/j.atmosenv.2010.09.055

Ram, K., Sarin, M.M. (2015). Atmospheric carbonaceous aerosols from Indo-Gangetic Plain and Central Himalaya: Impact of anthropogenic sources. J. Environ. Manage. 148, 153–163. https://doi.org/10.1016/j.jenvman.2014.08.015

Ramana, M.V., Ramanathan, V., Feng, Y., Yoon, S.C., Kim, S.W., Carmichael, G.R., Schauer, J.J. (2010). Warming influenced by the ratio of black carbon to sulphate and the black-carbon source. Nat. Geosci. 3, 542–545. https://doi.org/10.1038/ngeo918

Ramanathan, V., Carmichael, G. (2008). Global and regional climate changes due to black carbon. Nat. Geosci. 1, 221–227. https://doi.org/10.1038/ngeo156

Ramgolam, K., Favez, O., Cachier, H., Gaudichet, A., Marano, F., Martinon, L., Baeza-Squiban, A. (2009). Size-partitioning of an urban aerosol to identify particle determinants involved in the proinflammatory response induced in airway epithelial cells. Part. Fibre Toxicol. 6, 10. https://doi.org/10.1186/1743-8977-6-10

Rastogi, N., Sarin, M.M. (2006). Chemistry of aerosols over a semi-arid region: Evidence for acid neutralization by mineral dust. Geophys. Res. Lett. 33, L23815. https://doi.org/10.1029/2006GL027708

Rastogi, N., Singh, A., Sarin, M.M., Singh, D. (2016). Temporal variability of primary and secondary aerosols over northern India: Impact of biomass burning emissions. Atmos. Environ. 125, 396–403. https://doi.org/10.1016/j.atmosenv.2015.06.010

Rengarajan, R., Sarin, M.M., Sudheer, A.K. (2007). Carbonaceous and inorganic species in atmospheric aerosols during wintertime over urban and high-altitude sites in North India. J. Geophys. Res. 112, D21307. https://doi.org/10.1029/2006JD008150

Saarikoski, S., Timonen, H., Saarnio, K., Aurela, M., Järvi, L., Keronen, P., Kerminen, V.M., Hillamo, R. (2008). Sources of organic carbon in fine particulate matter in northern European urban air. Atmos. Chem. Phys. 8, 6281–6295. https://doi.org/10.5194/acp-8-6281-2008

Sagar, R., Dumka, U.C., Naja, M., Singh, N., Phanikumar, D.V. (2015). ARIES, Nainital: A strategically important location for climate change studies in the Central Gangetic Himalayan region. Curr. Sci. 109, 703–715. http://prints.iiap.res.in/handle/2248/7089

Sahu, RK, Pervez, S., Chow, J.C., Watson, J.G., Tiwari, S., Panicker, A.S., Chakrabarty, R.K., Pervez, YF (2018). Temporal and spatial variations of PM$_{2.5}$ organic and elemental carbon in Central India. Environ. Geochem. Health 40, 2205–2222. https://doi.org/10.1007/s10653-018-0093-0

Salma, I., Chi, X., Maenhaut, W. (2004). Elemental and organic carbon in urban canyon and background environments in Budapest, Hungary. Atmos. Environ. 38, 27–36. https://doi.org/10.1016/j.atmosenv.2003.09.047

Sandradewi, J., Prevot, A., Szidat, S., Perron, N., Alfarra, M., Lanz, V., Weingartner, E., Baltensperger, U. (2008). Using Aerosol light absorption measurements for the quantitative determination of wood burning and traffic emission contributions to particulate matter. Environ. Sci. Technol. 42, 3316–3323. https://doi.org/10.1021/es702253m

Sarkar, C., Chatterjee, A., Majumdar, D., Ghosh, S.K., Srivastava, A., Raha, S. (2014). Volatile organic compounds over Eastern Himalaya, India: Temporal variation and source characterization using Positive Matrix Factorization. Atmos. Chem. Phys. Discus. 14, 32133–32175. https://doi.org/10.5194/acpd-14-32133-2014

Sarkar, C., Chatterjee, A., Singh, A.K., Ghosh, S.K., Raha, S. (2015). Characterization of black carbon aerosols over Darjeeling—A high altitude Himalayan station in eastern India. Aerosol Air Qual. Res. 15, 465–478. https://doi.org/10.4209/aaqr.2014.02.0028

Sen, A., Karapurkar, S., Saxena, M., Shenoy, D.M., Chaterjee, A., Choudhuri, A., Das, T., Khan, A.,

Kuniyal, J.C., Pal, S., Singh, D., Sharma, S.K., Kotnala, R.K., Mandal, T. (2018). Stable carbon and nitrogen isotopic composition of PM_{10} over Indo-Gangetic Plains (IGP), adjoining regions and Indo-Himalayan Range (IHR) during a winter 2014 campaign. Environ. Sci. Pollut. Res. 25, 26279–26296. https://doi.org/10.1007/s11356-018-2567-0

Sharma, S.K., Mandal, T., Sharma, C., Kuniyal, J.C., Joshi, R., Dhyani, P., Garhwal, R., Sen, A., Ghayas, H., Gupta, N., Sharma, P., Saxena, M., Sharma, A., Arya, B., Kumar, A. (2014a). Measurements of particulate ($PM_{2.5}$), BC and trace gases over the northwestern Himalayan region of India. MAPAN 29, 243–253. https://doi.org/10.1007/s12647-014-0104-2

Sharma, S.K., Mandal, T.K., Saxena, M., Rashmi, Sharma, A., Datta, A., Saud, T. (2014b). Variation of OC, EC, WSIC and trace metals of PM_{10} in Delhi, India. J. Atmos. Sol. Terr. Phys. 113, 10–22. https://doi.org/10.1016/j.jastp.2014.02.008

Sharma, S.K., Agarwal, P., Mandal, T., Karapurkar, S., Shenoy, D.M., Peshin, S.K., Gupta, A., Saxena, M., Jain, S., Sharma, A., Yadav, S. (2017). Study on ambient air quality of megacity Delhi, India during odd–even strategy. MAPAN 32, 155–165. https://doi.org/10.1007/s12647-016-0201-5

Sharma, S.K., Mandal, T., De, A.K., Deb, N., Jain, S., Saxena, M., Pal, S., Choudhuri, A.K., Yadav, S. (2018). Carbonaceous and inorganic species in PM_{10} during wintertime over Giridih, Jharkhand (India). J. Atmos. Chem. 75, 219–233. https://doi.org/10.1007/s10874-017-9373-9

Sharma, S.K., Choudhary, N., Kotnala, G., Das, D., Mukherjee, S., Ghosh, A., Vijayan, N., Rai, A., Chatterjee, A., Mandal, T.K. (2020a). Wintertime carbonaceous species and trace metals in PM_{10} in Darjeeling: A high altitude town in the eastern Himalayas. Urban Clim. 34, 100668. https://doi.org/10.1016/j.uclim.2020.100668

Sharma, S.K., Choudhary, N., Srivastava, P., Naja, M., Vijayan, N., Kotnala, G., Mandal, T. (2020b). Variation of carbonaceous species and trace elements in PM_{10} at a mountain site in the central Himalayan region of India. J. Atmos. Chem. 77, 1–14. https://doi.org/10.1007/s10874-020-09402-9

Sharma, S.K., Mukherjee, S., Choudhary, N., Rai, A., Ghosh, A., Chatterjee, A., Vijayan, N., Mandal, T. (2021). Seasonal variation and sources of carbonaceous species and elements in $PM_{2.5}$ and PM_{10} over the eastern Himalaya. Environ. Sci. Pollut. Res. 28, 51642–51656. https://doi.org/10.1007/s11356-021-14361-z

Sheoran, R., Dumka, U.C., Kaskaoutis, D.G., Grivas, G., Ram, K., Prakash, J., Hooda, R.K., Tiwari, R.K., Mihalopoulos, N. (2021). Chemical composition and source apportionment of total suspended particulate in the central Himalayan region. Atmosphere 12, 1128. https://doi.org/10.3390/atmos12091228

Shivani, Gadi, R., Sharma, S.K., Mandal, T.K. (2019). Seasonal variation, source apportionment and source attributed health risk of fine carbonaceous aerosols over National Capital Region, India. Chemosphere 237, 124500. https://doi.org/10.1016/j.chemosphere.2019.124500

Shridhar, V., Khillare, P.S., Agarwal, T., Ray, S. (2009). Metallic species in ambient particulate matter at rural and urban location of Delhi. J. Hazard. Mater. 175, 600–607. https://doi.org/10.1016/j.jhazmat.2009.10.047

Shrivastav, R. (2001). Atmospheric heavy metal pollution. Resonance 6, 62–68. https://doi.org/10.1007/BF02994594

Singh, N., Banerjee, T., Raju, M.P., Deboudt, K., Sorek-Hamer, M., Singh, R.S., Mall, R. (2018). Aerosol chemistry, transport, and climatic implications during extreme biomass burning emissions over the Indo-Gangetic Plain. Atmos. Chem. Phys. 18, 14197–14215. https://doi.org/10.5194/acp-18-14197-2018

Song, Y., Zhang, Y., Xie, S., Zeng, L., Zheng, M., Salmon, L., Shao, M., Slanina, S. (2006). Source apportionment of $PM_{2.5}$ in Beijing by positive matrix factorization. Atmos. Environ. 40, 1526–1537. https://doi.org/10.1016/j.atmosenv.2005.10.039

Soni, A., Kumar, U., Prabhu, V., Shridhar, V. (2020). Characterization, source apportionment and carcinogenic risk assessment of atmospheric particulate matter at Dehradun, situated in the foothills of Himalayas. J. Atmos. Sol. Terr. Phys. 199, 105205. https://doi.org/10.1016/j.jastp.2020.105205

Srinivas, B., Sarin, M.M. (2014). $PM_{2.5}$, EC and OC in atmospheric outflow from the Indo-Gangetic Plain: Temporal variability and aerosol organic carbon-to-organic mass conversion factor. Sci. Total Environ. 487, 196–205. https://doi.org/10.1016/j.scitotenv.2014.04.002

Streets, D., Yarber, K., Woo, J.H., Carmichael, G. (2003). Biomass burning in Asia: Annual and
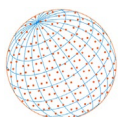
seasonal estimates and atmospheric emissions. Global Biogeochem. Cycles 17. https://doi.org/10.1029/2003GB002040

Sudheer, A.K., Sarin, M.M. (2008). Carbonaceous aerosols in MABL of Bay of Bengal: Influence of continental outflow. Atmos. Environ. 42, 4089–4100. https://doi.org/10.1016/j.atmosenv.2008.01.033

Taylor, S.R., McLennan, S.M. (1995). The geochemical evolution of the continental crust. Rev. Geophys. 33, 241–265. https://doi.org/10.1029/95RG00262

Thurston, G., Spengler, J. (1985). A quantitative assessment of source contributions to inhalable particulate matter pollution in metropolitan Boston. Atmos. Environ. 19, 9–25. https://doi.org/10.1016/0004-6981(85)90132-5

Tsai, D.H., Amyai, N., Marques-Vidal, P., Wang, J.L., Riediker, M., Mooser, V., Paccaud, F., Waeber, G., Vollenweider, P., Bochud, M. (2012). Effects of particulate matter on inflammatory markers in the general adult population. Part. Fibre Toxicol. 9, 24–24. https://doi.org/10.1186/1743-8977-9-24

Wang, Y., Pavuluri, C.M., Fu, P., Li, P., Dong, Z., Xu, Z., Ren, H., Fan, Y., Li, L., Zhang, Y.L., Liu, C.Q. (2019). Characterization of secondary organic aerosol tracers over Tianjin, North China during summer to autumn. ACS Earth Space Chem. 3, 2339–2352. https://doi.org/10.1021/acsearthspacechem.9b00170

Xu, J., Wang, Q., Deng, C., McNeill, V.F., Fankhauser, A., Wang, F., Zheng, X., Shen, J., Huang, K., Zhuang, G. (2018). Insights into the characteristics and sources of primary and secondary organic carbon: High time resolution observation in urban Shanghai. Environ. Pollut. 233, 1177–1187. https://doi.org/10.1016/j.envpol.2017.10.003

Yadav, S., Tandon, A., Attri, A.K. (2013). Monthly and seasonal variations in aerosol associated n-alkane profiles in relation to meteorological parameters in New Delhi, India. Aerosol Air Qual. Res. 13, 287–300. https://doi.org/10.4209/aaqr.2012.01.0004

Yang, J., Ji, Z., Kang, S., Tripathee, L. (2021). Contribution of south Asian biomass burning to black carbon over the Tibetan Plateau and its climatic impact. Environ. Pollut. 270, 116195. https://doi.org/10.1016/j.envpol.2020.116195

Yang, W., Wang, G., Bi, C. (2017). Analysis of long-range transport effects on $PM_{2.5}$ during a short severe haze in Beijing, China. Aerosol Air Qual. Res. 17, 1610–1622. https://doi.org/10.4209/aaqr.2016.06.0220

Yuan, Q., Wan, X., Cong, Z., Li, M., Liu, L., Shu, S., Liu, R., Xu, L., Zhang, J., Ding, X., Li, W. (2020). In situ observations of light-absorbing carbonaceous aerosols at Himalaya: Analysis of the south Asian sources and trans-Himalayan valleys transport pathways. J. Geophys. Res. 125, e2020JD032615. https://doi.org/10.1029/2020JD032615

Yuan, Q., Xu, J., Liu, L., Zhang, A., Liu, Y., Zhang, J., Wan, X., Li, M., Qin, K., Cong, Z., Wang, Y., Kang, S., Shi, Z., Pósfai, M., Li, W. (2021). Evidence for large amounts of brown carbonaceous tarballs in the Himalayan atmosphere. Environ. Sci. Technol. Lett. 8, 16–23. https://doi.org/10.1021/acs.estlett.0c00735

Zhang, Y., Schauer, J. J., Zhang, Y., Zeng, L., Wei, Y., Liu, Y., Shao, M. (2008). Characteristics of particulate carbon emissions from real-world Chinese coal combustion. Environ. Sci. Technol. 42, 5068–5073. https://doi.org/10.1021/es7022576

Zheng, J., Hu, M., Du, Z., Shang, D., Gong, Z., Qin, Y., Fang, J., Gu, F., Li, M., Peng, J., Li, J., Zhang, Y., Huang, X., He, L., Wu, Y., Guo, S. (2017). Influence of biomass burning from South Asia at a high-altitude mountain receptor site in China. Atmos. Chem. Phys. 17, 6853–6864. https://doi.org/10.5194/acp-17-6853-2017